

# Three newly-discovered sub-Jupiter-mass planets: WASP-69b & WASP-84b transit active K dwarfs and WASP-70Ab transits the evolved primary of a G4+K3 binary<sup>\*†</sup>

D. R. Anderson,<sup>1‡</sup> A. Collier Cameron,<sup>2</sup> L. Delrez,<sup>3</sup> A. P. Doyle,<sup>1</sup> F. Faedi,<sup>4</sup> A. Fumel,<sup>3</sup> M. Gillon,<sup>3</sup> Y. Gómez Maqueo Chew,<sup>4</sup> C. Hellier,<sup>1</sup> E. Jehin,<sup>3</sup> M. Lendl,<sup>5</sup> P. F. L. Maxted,<sup>1</sup> F. Pepe,<sup>5</sup> D. Pollacco,<sup>4</sup> D. Queloz,<sup>5,6</sup> D. Ségransan,<sup>5</sup> I. Skillen,<sup>7</sup> B. Smalley,<sup>1</sup> A. M. S. Smith,<sup>1,8</sup> J. Southworth,<sup>1</sup> A. H. M. J. Triaud,<sup>5,9</sup> O. D. Turner,<sup>1</sup> S. Udry<sup>5</sup> and R. G. West<sup>4</sup>

<sup>1</sup>*Astrophysics Group, Keele University, Staffordshire ST5 5BG, UK.*

<sup>2</sup>*SUPA, School of Physics and Astronomy, University of St. Andrews, North Haugh, Fife KY16 9SS, UK*

<sup>3</sup>*Institut d'Astrophysique et de Géophysique, Université de Liège, Allée du 6 Août, 17, Bat. B5C, Liège 1, Belgium*

<sup>4</sup>*Department of Physics, University of Warwick, Coventry CV4 7AL, UK*

<sup>5</sup>*Observatoire de Genève, Université de Genève, 51 Chemin des Maillettes, 1290 Sauverny, Switzerland*

<sup>6</sup>*Cavendish Laboratory, J J Thomson Avenue, Cambridge, CB3 0HE, UK*

<sup>7</sup>*Isaac Newton Group of Telescopes, Apartado de Correos 321, E-38700 Santa Cruz de la Palma, Tenerife, Spain*

<sup>8</sup>*N. Copernicus Astronomical Centre, Polish Academy of Sciences, Bartycka 18, 00-716, Warsaw, Poland*

<sup>9</sup>*Department of Physics, and Kavli Institute for Astrophysics and Space Research, Massachusetts Institute of Technology, Cambridge, MA 02139, USA.*

Accepted 2014 August 22. Received 2014 August 18; in original form 2013 October 21

## ABSTRACT

We report the discovery of the transiting exoplanets WASP-69b, WASP-70Ab and WASP-84b, each of which orbits a bright star ( $V \sim 10$ ). WASP-69b is a bloated Saturn-mass planet ( $0.26 M_{\text{Jup}}$ ,  $1.06 R_{\text{Jup}}$ ) in a 3.868-d period around an active,  $\sim 1$ -Gyr, mid-K dwarf. ROSAT detected X-rays  $60 \pm 27''$  from WASP-69. If the star is the source then the planet could be undergoing mass-loss at a rate of  $\sim 10^{12} \text{ g s}^{-1}$ . This is 1–2 orders of magnitude higher than the evaporation rate estimated for HD 209458b and HD 189733b, both of which have exhibited anomalously-large Lyman- $\alpha$  absorption during transit. WASP-70Ab is a sub-Jupiter-mass planet ( $0.59 M_{\text{Jup}}$ ,  $1.16 R_{\text{Jup}}$ ) in a 3.713-d orbit around the primary of a spatially-resolved, 9–10-Gyr, G4+K3 binary, with a separation of  $3''.3$  ( $\geq 800$  AU). WASP-84b is a sub-Jupiter-mass planet ( $0.69 M_{\text{Jup}}$ ,  $0.94 R_{\text{Jup}}$ ) in an 8.523-d orbit around an active,  $\sim 1$ -Gyr, early-K dwarf. Of the transiting planets discovered from the ground to date, WASP-84b has the third-longest period. For the active stars WASP-69 and WASP-84, we pre-whitened the radial velocities using a low-order harmonic series. We found this reduced the residual scatter more than did the oft-used method of pre-whitening with a fit between residual radial velocity and bisector span. The system parameters were essentially unaffected by pre-whitening.

**Key words:** planets and satellites: detection – techniques: photometric – techniques: radial velocities – planets and satellites: individual: WASP-69b – planets and satellites: individual: WASP-70Ab – planets and satellites: individual: WASP-84b.

## 1 INTRODUCTION

Radial-velocity (RV) surveys tend to focus on inactive stars because of the inherent difficulty in determining whether the source of an RV signal is stellar activity or reflex motion induced by an orbiting body (e.g. Queloz et al. 2001; Santos et al. 2003; Desidera et al. 2004; Huélamo et al. 2008). Transit surveys are not affected by

\* Based on observations made with the WASP-South (South Africa) and SuperWASP-North (La Palma) photometric survey instruments, the RISE camera on the 2-m Liverpool Telescope under program PL12B13, and, all located at La Silla: the 60-cm TRAPPIST photometer, EulerCam and the CORALIE spectrograph, both mounted on the 1.2-m Euler-Swiss telescope, and the HARPS spectrograph on the ESO 3.6-m telescope under program 89.C-0151.

† The photometric time-series and radial-velocity data used in this work are available at the CDS via any-

mous ftp to cdsarc.u-strasbg.fr (130.79.128.5) or via <http://cdsarc.u-strasbg.fr/viz-bin/qcat?J/MNRAS/445/1114>  
‡ E-mail: d.r.anderson@keele.ac.uk

this ambiguity as stellar activity does not produce transit-like features in lightcurves. The separation of the RV contributions due to reflex motion from those due to activity can prove simple or unnecessary in the case of short-period, giant transiting planets (e.g. Maxted et al. 2011; Anderson et al. 2012), but it is non-trivial for lower mass planets such as the super-Earth CoRoT-7b (Queloz et al. 2009; Lanza et al. 2010; Pont, Aigrain & Zucker 2011; Ferraz-Mello et al. 2011; Hatzes et al. 2011).

Transiting planets orbiting one component of a multiple system have been known for some time (e.g. WASP-8; Queloz et al. 2010) and the *Kepler* mission recently found circumbinary transiting planets (e.g. Kepler-16 and Kepler-47; Doyle et al. 2011; Orosz et al. 2012). For those systems with a spatially-resolved secondary of similar brightness to the primary (e.g. WASP-77; Maxted et al. 2013), the secondary can be used as the reference source in ground-based observations of exoplanet atmospheres. Without a suitable reference such observations tend to either fail to reach the required precision or give ambiguous results (e.g. Swain et al. 2010; Mandell et al. 2011; Angerhausen & Krabbe 2011).

The longitudinal coverage of ground-based transit surveys such as HAT-Net and HAT-South makes them relatively sensitive to longer-period planets (Bakos et al. 2004, 2013). For example, in the discovery of HAT-P-15b, the planet with the longest period (10.9 d) of those found by ground-based transit surveys, transits were observed asynchronously from Arizona and Hawai'i (Kovács et al. 2010). By combining data from multiple seasons, surveys such as SuperWASP can increase their sensitivity to longer periods without additional facility construction costs (Pollacco et al. 2006).

We report here the discovery of three exoplanet systems, each comprising of a giant planet transiting a bright host star ( $V \sim 10$ ). WASP-69b is a bloated Saturn-mass planet in a 3.868-d period around an active mid-K dwarf. WASP-70Ab is a sub-Jupiter-mass planet in a 3.713-d orbit around the primary of a spatially-resolved G4+K3 binary. WASP-84b is a sub-Jupiter-mass planet in an 8.523-d orbit around an active early-K dwarf. In Section 2 we report the photometric and spectroscopic observations leading to the identification, confirmation and characterisation of the exoplanet systems. In Section 3 we present spectral analyses of the host stars and, in Section 4, searches of the stellar lightcurves for activity-rotation induced modulation. In Section 5 we detail the derivation of the systems' parameters from combined analyses. We present details of each system in Sections 6, 7 and 8 and, finally, we summarise our findings in Section 9.

## 2 OBSERVATIONS

The WASP (Wide Angle Search for Planets) photometric survey (Pollacco et al. 2006) monitors bright stars ( $V = 8-15$ ) using two eight-camera arrays, each with a field of view of 450 deg<sup>2</sup>. Each array observes up to eight pointings per night with a cadence of 5–10 min, and each pointing is followed for around five months per season. The WASP-South station (Hellier et al. 2011) is hosted by the South African Astronomical Observatory and the SuperWASP-North station (Faedi et al. 2011) is hosted by the Isaac Newton Group in the Observatorio del Roque de Los Muchachos on La Palma.

The WASP data were processed and searched for transit signals as described in Collier Cameron et al. (2006) and the candidate selection process was performed as described in Collier Cameron et al. (2007). We perform a search for transits on

each season of data from each camera separately and we perform combined searches on all WASP data available on each star, allowing for photometric offsets between datasets. This results in early detection, a useful check for spurious signals and increased sensitivity to shallow transits and long periods. We routinely correct WASP data for systematic effects using a combination of SYSREM and TFA (Tamuz, Mazeh & Zucker 2005; Kovács, Bakos & Noyes 2005). TFA is more effective at e.g. removing sinusoidal modulation, as can result from a non-axisymmetric distribution of star spots, which can otherwise swamp the transit signal. However, TFA tends to suppress transits whereas SYSREM does not. Therefore we use SYSREM-detrended WASP lightcurves, corrected for modulation as necessary, in system characterisation (Sections 4 and 5).

We detected periodic dimmings in the WASP lightcurves of WASP-69, -70 and -84 with periods of 3.868 d, 3.713 d and 8.523 d, respectively. We identified WASP-69b and WASP-70Ab as candidates based on data from the 2008 season alone, whereas data from two seasons (2009 and 2010) were required to pick up the longer-period WASP-84b. This highlights the importance of multi-epoch coverage for sensitivity to longer-period systems. The number of full/partial transits observed of WASP-69b was 2/2 in 2008, 2/5 in 2009 and 2/4 in 2010. The figures for WASP-70Ab are 4/2 in 2008, 2/5 in 2009 and 2/2 in 2010. The figures for WASP-84b are 1/1 in 2009, 1/2 in 2010 and 2/0 in 2011. In the top panels of Figures 1, 2 and 3 we plot all available WASP data, phase-folded on the best-fitting periods (Section 5) and corrected for systematics with SYSREM; the lightcurves of WASP-69 and WASP-84 have been corrected for rotation modulation (Section 4). Coherent structure is apparent in the lightcurve of WASP-84 with a timescale of  $\sim 1$  day. This is probably due to an imperfect subtraction of the rotational modulation signal and it does not appear to affect the transit (see the second panel of Figure 3). Though the structure is far reduced in a lightcurve detrended with SYSREM+TFA (not shown), we opted not to use it as the transit was also suppressed (as was evident from a combined analysis including the RISE lightcurves).

We obtained spectra of each star using the CORALIE spectrograph mounted on the Euler-Swiss 1.2-m telescope. Two spectra of WASP-84 from 2011 Dec 27 and 2012 Jan 2 were discarded as they were taken through cloud. We also obtained five spectra of WASP-70A with the HARPS spectrograph mounted on the ESO 3.6-m telescope. As the diameter of the HARPS fibre is half that of the CORALIE fibre (1'' cf. 2'') this is a useful check for contamination of the CORALIE spectra by WASP-70B, located  $\sim 3''$  away. Radial-velocity (RV) measurements were computed by weighted cross-correlation (Baranne et al. 1996; Pepe et al. 2005) with a numerical G2-spectral template for WASP-70 and with a K5-spectral template for both WASP-69 and WASP-84 (Table 3). RV variations were detected with periods similar to those found from the WASP photometry and with semi-amplitudes consistent with planetary-mass companions. The RVs are plotted, phased on the transit ephemerides, in the third panel of Figures 1, 2 and 3.

For each star, we tested the hypothesis that the RV variations are due to spectral-line distortions caused by a blended eclipsing binary or starspots by performing a line-bisector analysis of the cross-correlation functions (Queloz et al. 2001). The lack of correlation between bisector span and RV supports our conclusion that the periodic dimming and RV variation of each system are instead caused by a transiting planet (fourth panel of Figures 1, 2 and 3).

We performed high-quality transit observations to refine the systems' parameters using the 0.6-m TRAPPIST robotic telescope (Gillon et al. 2011; Jehin et al. 2011), EulerCam mounted on the

1.2-m Swiss Euler telescope (Lendl et al. 2012), and the RISE camera mounted on the 2-m Liverpool Telescope (Steele et al. 2004, 2008). Lightcurves, extracted from the images using standard aperture photometry, are displayed in the second panel of Figures 1, 2 and 3 and the data are provided in Table 4. The RISE camera was specifically designed to obtain high-precision, high-cadence transit lightcurves and the low scatter of the WASP-84b transits demonstrate the instrument’s aptness (see Figure 3).

A summary of observations is given in Table 1 and the data are plotted in Figures 1, 2 and 3. The WASP photometry, the radial-velocity measurements and the high signal-to-noise transit photometry are provided in tables online at the CDS; a guide to their content and format is given in Tables 2, 3 and 4.

### 3 STELLAR PARAMETERS FROM SPECTRA

The CORALIE spectra were co-added for each star to produce high-SNR spectra for analysis using the methods of Gillon et al. (2009) and Doyle et al. (2013). We obtained an initial estimate of effective temperature ( $T_{\text{eff}}$ ) from the  $H_{\alpha}$  line, then refined the determination using excitation balance of the Fe I abundance. The surface gravity ( $\log g_*$ ) was determined from the Ca I lines at 6162 and 6439 (Bruntt et al. 2010b), along with the Na I D and Mg I b lines. The elemental abundances were determined from equivalent-width measurements of several clean and unblended lines. A value for microturbulence ( $\xi_t$ ) was determined from Fe I using the method of Magain (1984). The quoted error estimates include that given by the uncertainties in  $T_{\text{eff}}$ ,  $\log g_*$  and  $\xi_t$ , as well as the scatter due to measurement and atomic data uncertainties.

We determined the projected stellar rotation velocity ( $v \sin I$ ) by fitting the profiles of several unblended Fe I lines. We took macroturbulence values of  $2.3 \pm 0.3 \text{ km s}^{-1}$  for WASP-70A and  $1.2 \pm 0.3 \text{ km s}^{-1}$  for WASP-84 from the tabulation of Bruntt et al. (2010a). For WASP-69 and WASP-70B we assumed macroturbulence to be zero, since for mid-K stars it is expected to be lower than that of thermal broadening (Gray 2008). An instrumental FWHM of  $0.11 \pm 0.01$  was determined from the telluric lines around 6300.

The results of the spectral analysis are given in Table 5 and further details of each star are given in Sections 6, 7 and 8.

### 4 STELLAR ROTATION FROM LIGHTCURVE MODULATION

We analysed the WASP lightcurves of each star to determine whether they show periodic modulation due to the combination of magnetic activity and stellar rotation. We used the sine-wave fitting method described in Maxted et al. (2011) to calculate periodograms such as those shown in Figures 4 and 5. The false alarm probability levels shown in these figures are calculated using a boot-strap Monte Carlo method also described in Maxted et al. (2011).

Variability due to star spots is not expected to be coherent on long timescales as a consequence of the finite lifetime of star-spots and differential rotation in the photosphere so we analysed each season of data separately. We also analysed the data from each WASP camera separately as the data quality can vary between cameras. We removed the transit signal from the data prior to calculating the periodograms by subtracting a simple transit model from the lightcurve. We then calculated periodograms over 4096 uniformly spaced frequencies from 0 to 1.5 cycles  $\text{day}^{-1}$ .

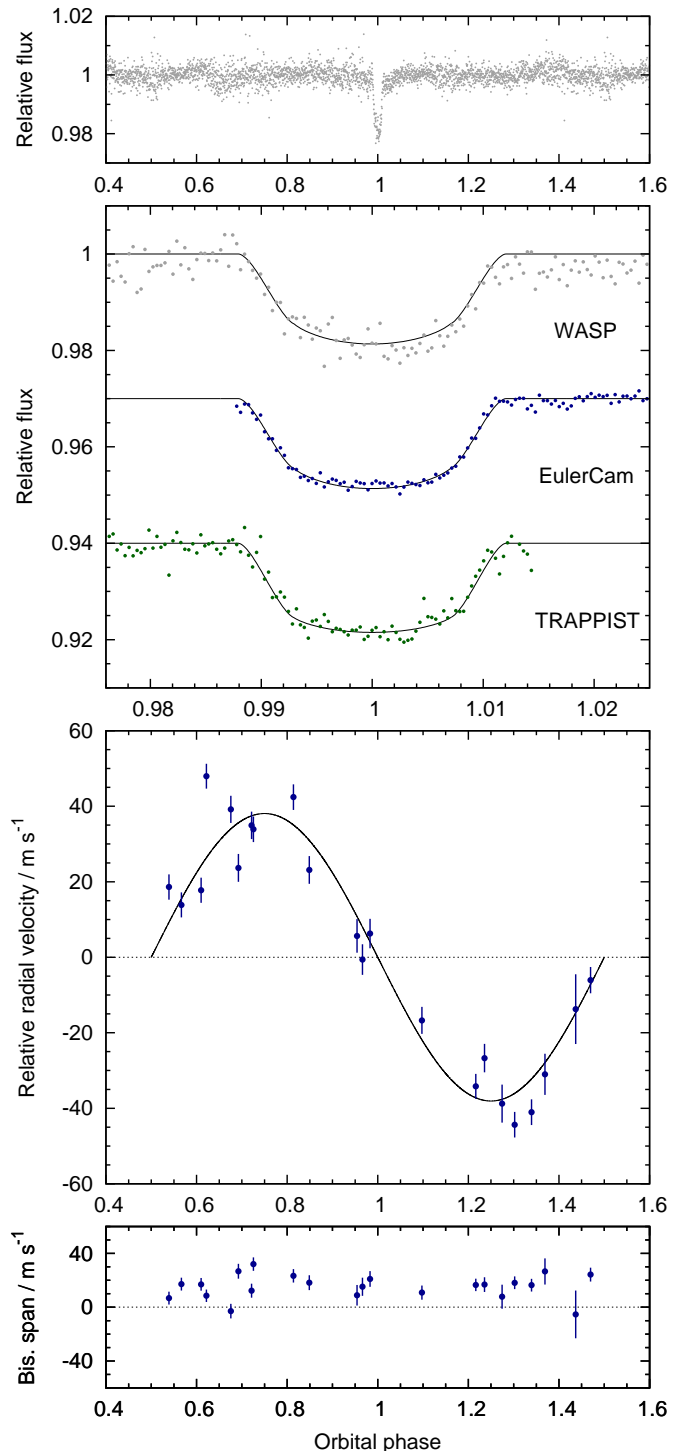


**Figure 1.** WASP-69b discovery data. Top panel: WASP lightcurve folded on the transit ephemeris and binned in phase with a bin-width,  $\Delta\phi$ , equivalent to two minutes. Second panel: Transit lightcurves from facilities as labelled, offset for clarity and binned with  $\Delta\phi = 2$  minutes. The best-fitting transit model is superimposed. Third panel: The pre-whitened CORALIE radial velocities with the best-fitting circular Keplerian orbit model. Bottom panel: The absence of any correlation between bisector span and radial velocity excludes transit mimics.

**Table 1.** Summary of observations

| Facility            | Date                    | $N_{\text{obs}}$ | $T_{\text{exp}}$<br>(s) | Filter             |
|---------------------|-------------------------|------------------|-------------------------|--------------------|
| <b>WASP-69:</b>     |                         |                  |                         |                    |
| WASP-South          | 2008 Jun–2010 Oct       | 29 800           | 30                      | Broad (400–700 nm) |
| SuperWASP-North     | 2008 Jun–2009 Oct       | 22 600           | 30                      | Broad (400–700 nm) |
| Euler/CORALIE       | 2009 Aug–2011 Sep       | 22               | 1800                    | Spectroscopy       |
| Euler/EulerCam      | 2011 Nov 10             | 367              | ~30                     | Gunn- <i>r</i>     |
| TRAPPIST            | 2012 May 21             | 873              | ~10                     | $z'$               |
| <b>WASP-70 A+B:</b> |                         |                  |                         |                    |
| WASP-South          | 2008 Jun–2009 Oct       | 12 700           | 30                      | Broad (400–700 nm) |
| SuperWASP-North     | 2008 Sep–2010 Oct       | 14 000           | 30                      | Broad (400–700 nm) |
| A: Euler/CORALIE    | 2009 Jul–2011 Oct       | 21               | 1800                    | Spectroscopy       |
| A: ESO-3.6m/HARPS   | 2012 Jun 26–2012 Jul 07 | 5                | 600–1800                | Spectroscopy       |
| B: Euler/CORALIE    | 2009 Sep 15–22          | 4                | 1800                    | Spectroscopy       |
| Euler/EulerCam      | 2011 Sep 20             | 466              | ~40                     | Gunn- <i>r</i>     |
| TRAPPIST            | 2011 Sep 20             | 1334             | ~12                     | $I + z'$           |
| <b>WASP-84:</b>     |                         |                  |                         |                    |
| WASP-South          | 2009 Jan–2011 Apr       | 14 100           | 30                      | Broad (400–700 nm) |
| SuperWASP-North     | 2009 Dec–2011 Mar       | 8 700            | 30                      | Broad (400–700 nm) |
| Euler/CORALIE       | 2011 Dec–2012 Mar       | 20               | 1800                    | Spectroscopy       |
| TRAPPIST            | 2012 Mar 01             | 557              | ~25                     | $z'$               |
| LT/RISE             | 2013 Jan 01             | 4322             | 4                       | $V + R$            |
| LT/RISE             | 2013 Jan 18             | 1943             | 8                       | $V + R$            |

**Table 2.** WASP photometry

| Set | Star    | Field       | Season | Camera | HJD(UTC)<br>–2450000<br>(day) | Mag., $M$ | $\sigma_M$ |
|-----|---------|-------------|--------|--------|-------------------------------|-----------|------------|
| 1   | WASP-69 | SW2045–0345 | 2008   | 223    | 4622.483160                   | 9.9086    | 0.0135     |
| 1   | WASP-69 | SW2045–0345 | 2008   | 223    | 4622.483588                   | 9.8977    | 0.0139     |
| ... |         |             |        |        |                               |           |            |
| 10  | WASP-70 | SW2114–1205 | 2008   | 221    | 4622.483391                   | 11.2161   | 0.0096     |
| 10  | WASP-70 | SW2114–1205 | 2008   | 221    | 4622.483831                   | 11.2098   | 0.0101     |
| ... |         |             |        |        |                               |           |            |
| 19  | WASP-84 | SW0846+0544 | 2011   | 226    | 5676.372824                   | 10.9244   | 0.0193     |
| 19  | WASP-84 | SW0846+0544 | 2011   | 226    | 5676.373264                   | 10.9379   | 0.0178     |

The measurements for WASP-70 include both WASP-70A and WASP-70B. The uncertainties are the formal errors (i.e. they have not been rescaled). This table is available in its entirety via the CDS.

**Table 3.** Radial velocity measurements

| Set | Star     | Spectrograph | BJD(UTC)<br>–2450000<br>(day) | RV<br>( $\text{km s}^{-1}$ ) | $\sigma_{\text{RV}}$<br>( $\text{km s}^{-1}$ ) | BS<br>( $\text{km s}^{-1}$ ) |
|-----|----------|--------------|-------------------------------|------------------------------|--|------------------------------|
| 1   | WASP-69  | CORALIE      | 5070.719440                   | –9.61358                     | 0.00369  | –0.02674                     |
| 1   | WASP-69  | CORALIE      | 5335.854399                   | –9.64619                     | 0.00376  | –0.01681                     |
| ... |          |              |                               |                              |  |                              |
| 2   | WASP-70A | CORALIE      | 5038.745436                   | –65.43271                    | 0.00840  | –0.03410                     |
| 2   | WASP-70A | CORALIE      | 5098.630404                   | –65.48071                    | 0.01411  | –0.01614                     |
| ... |          |              |                               |                              |  |                              |
| 4   | WASP-84  | CORALIE      | 6003.546822                   | –11.52073                    | 0.00822  | 0.03026                      |
| 4   | WASP-84  | CORALIE      | 6004.564579                   | –11.56112                    | 0.00661  | –0.00007                     |

The presented RVs have not been pre-whitened and the uncertainties are the formal errors (i.e. with no added jitter). The uncertainty on bisector span (BS) is  $2\sigma_{\text{RV}}$ . This table is available in its entirety via the CDS.

**Table 4.** EulerCam, TRAPPIST and RISE photometry

| Set | Star     | Imager   | Filter<br>-2450000<br>(day) | BJD(UTC)    | Rel. flux, $F$ | $\sigma_F$ |
|-----|----------|----------|-----------------------------|-------------|----------------|------------|
| 1   | WASP-69  | EulerCam | Gunn-r                      | 5845.489188 | 1.000769       | 0.000842   |
| 1   | WASP-69  | EulerCam | Gunn-r                      | 5845.489624 | 0.999093       | 0.000840   |
| ... |          |          |                             |             |                |            |
| 4   | WASP-70A | TRAPPIST | $I + z'$                    | 5825.48554  | 1.006661       | 0.002919   |
| 4   | WASP-70A | TRAPPIST | $I + z'$                    | 5825.48576  | 1.001043       | 0.002903   |
| ... |          |          |                             |             |                |            |
| 8   | WASP-84  | RISE     | $V + R$                     | 6311.743556 | 0.999610       | 0.001827   |
| 8   | WASP-84  | RISE     | $V + R$                     | 6311.743649 | 1.000331       | 0.001829   |

The flux values are differential and normalised to the out-of-transit levels. The contamination of the WASP-70A photometry by WASP-70B has been accounted for. The uncertainties are the formal errors (i.e. they have not been rescaled). This table is available in its entirety via the CDS.

**Table 5.** Stellar parameters from spectra

| Parameter                       | WASP-69   | WASP-70A      | WASP-70B   | WASP-84   |
|---------------------------------|---|---------------|--|---|
| $T_{\text{eff}}$ / K            | 4700 ± 50   | 5700 ± 80     | 4900 ± 200   | 5300 ± 100  |
| $\log g_*$                      | 4.5 ± 0.15  | 4.26 ± 0.09   | 4.5 ± 0.2  | 4.4 ± 0.1   |
| $\xi_t$ / km s <sup>-1</sup>    | 0.7 ± 0.2   | 1.1 ± 0.1     | 0.7 ± 0.2  | 1.0 ± 0.1   |
| $v \sin I$ / km s <sup>-1</sup> | 2.2 ± 0.4   | 1.8 ± 0.4     | 3.9 ± 0.8 <sup>a</sup>   | 4.1 ± 0.3   |
| $\log R'_{\text{HK}}$           | -4.54   | -5.23         |  | -4.43   |
| [Fe/H]                          | 0.15 ± 0.08   | -0.01 ± 0.06  |  | 0.00 ± 0.10   |
| [Mg/H]                          | ...   | 0.05 ± 0.04   |  | ...   |
| [Si/H]                          | 0.42 ± 0.12   | 0.15 ± 0.05   |  | 0.06 ± 0.07   |
| [Ca/H]                          | 0.15 ± 0.09   | 0.07 ± 0.10   |  | 0.15 ± 0.09   |
| [Sc/H]                          | 0.25 ± 0.10   | 0.15 ± 0.11   |  | -0.01 ± 0.14  |
| [Ti/H]                          | 0.21 ± 0.06   | 0.07 ± 0.04   |  | 0.09 ± 0.11   |
| [V/H]                           | 0.48 ± 0.15   | 0.02 ± 0.08   |  | 0.21 ± 0.12   |
| [Cr/H]                          | 0.18 ± 0.18   | 0.05 ± 0.04   |  | 0.08 ± 0.15   |
| [Mn/H]                          | 0.40 ± 0.07   | ...           |  | ...   |
| [Co/H]                          | 0.42 ± 0.06   | 0.10 ± 0.05   |  | 0.04 ± 0.04   |
| [Ni/H]                          | 0.29 ± 0.11   | 0.05 ± 0.05   |  | -0.02 ± 0.06  |
| $\log A(\text{Li})$             | < 0.05 ± 0.07                                       | < 1.20 ± 0.07 | < 0.71 ± 0.25  | < 0.12 ± 0.11                                       |
| Sp. Type <sup>b</sup>           | K5  | G4            | K3   | K0  |
| Age <sup>c</sup> / Gyr          | ~2  |               | 9–10   | ~1  |
| Distance / pc                   | 50 ± 10 pc  |               | 245 ± 20   | 125 ± 20  |
| Constellation                   | Aquarius  |               | Aquarius   | Hydra   |
| R.A. (J2000) <sup>d</sup>       | 21 <sup>h</sup> 00 <sup>m</sup> 06 <sup>s</sup> .19 |               | 21 <sup>h</sup> 01 <sup>m</sup> 54 <sup>s</sup> .48 <sup>f</sup> | 08 <sup>h</sup> 44 <sup>m</sup> 25 <sup>s</sup> .71 |
| Dec. (J2000) <sup>d</sup>       | -05°05'40".1  |               | -13°25'59".8 <sup>f</sup>  | +01°51'36".0  |
| $B^d$                           | 10.93 ± 0.06  |               | 11.75 ± 0.13 <sup>f</sup>  | 11.64 ± 0.10  |
| $V^d$                           | 9.87 ± 0.03   |               | 10.79 ± 0.08 <sup>f</sup>  | 10.83 ± 0.08  |
| $J^e$                           | 8.03 ± 0.02   |               | 10.00 ± 0.03 <sup>f</sup>  | 9.35 ± 0.03   |
| $H^e$                           | 7.54 ± 0.02   |               | 9.71 ± 0.04 <sup>f</sup>   | 8.96 ± 0.02   |
| $K^e$                           | 7.46 ± 0.02   |               | 9.58 ± 0.03 <sup>f</sup>   | 8.86 ± 0.02   |
| 2MASS J <sup>e</sup>            | 21000618-0505398                                    |               | 21015446-1325595 <sup>f</sup>                                    | 08442570+0151361                                    |

<sup>a</sup> Due to low S/N, the  $v \sin I$  value for WASP-70B should be considered an upper limit.

<sup>b</sup> The spectral types were estimated from  $T_{\text{eff}}$  using the table in Gray (2008).

<sup>c</sup> See Sections 6, 7 and 8.

<sup>d</sup> From the Tycho-2 catalogue (Høg et al. 2000).

<sup>e</sup> From the Two Micron All Sky Survey (2MASS; Skrutskie et al. 2006).

<sup>f</sup> WASP-70A+B appear as a single entry in the Tycho-2 and 2MASS catalogues.

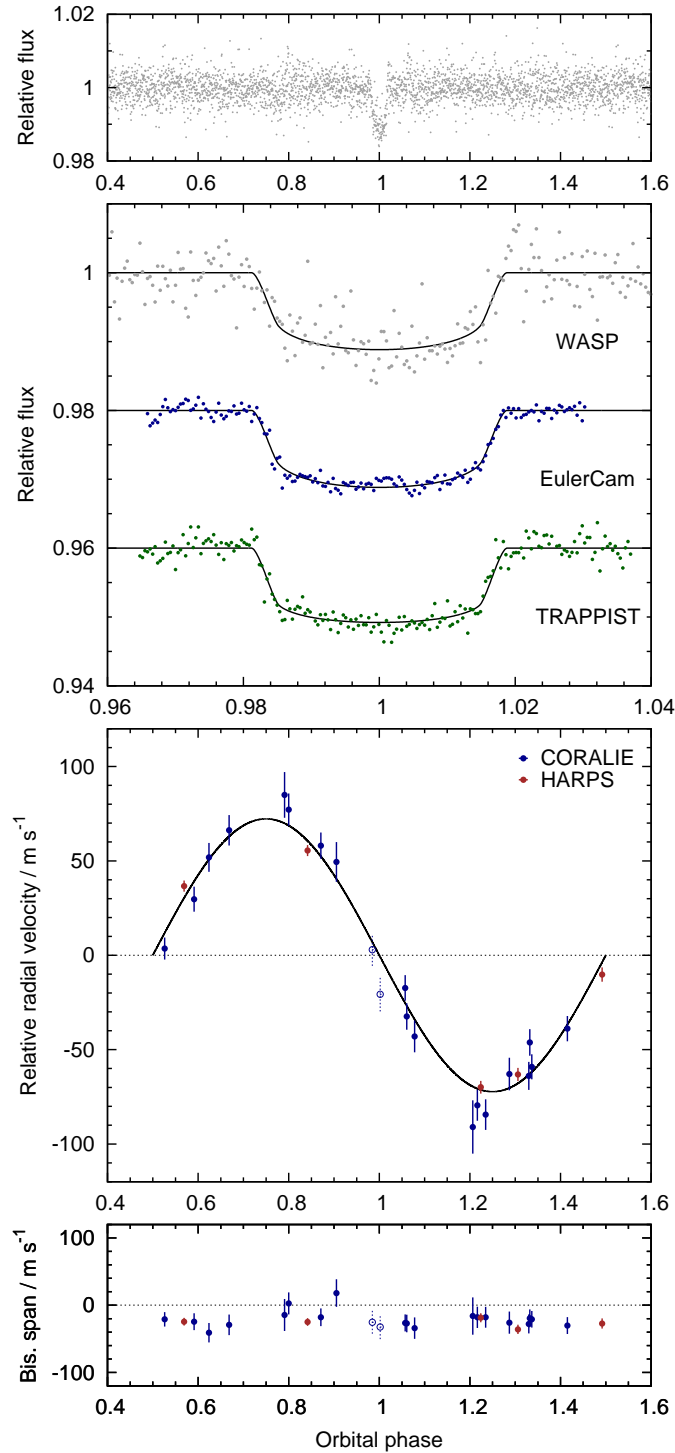


**Figure 2.** WASP-70Ab discovery data. Caption as for Figure 1. Two CORALIE RVs, taken during transit and depicted with open circles, were excluded from the fit as we did not model the Rossiter-McLaughlin effect. The RVs were not pre-whitened as we did not find WASP-70A to be active.

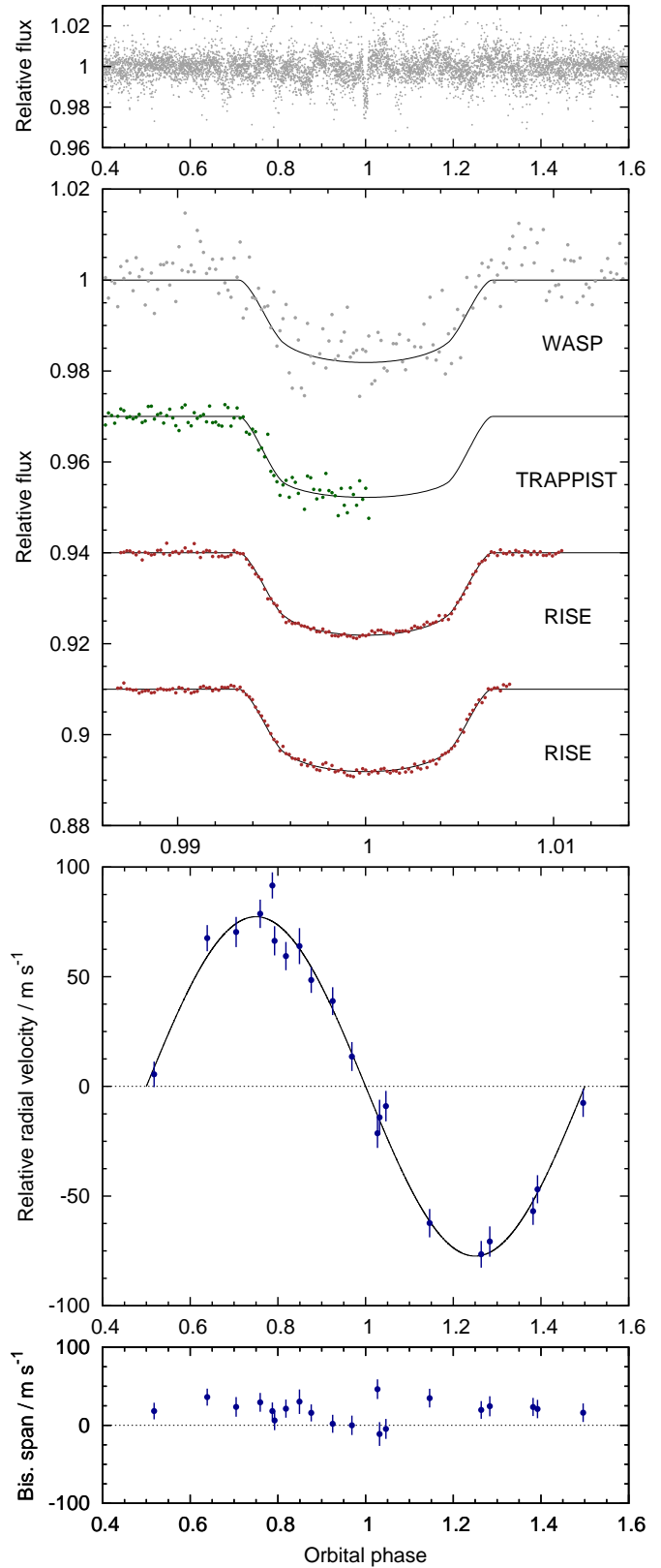


**Figure 3.** WASP-84b discovery data. Caption as for Figure 1.

We found no evidence of modulation above the 1-mmag level in the WASP-70A+B lightcurves. The results for WASP-69 and WASP-84 are shown in Table 6. Taking the average of the periods for each star gives our best estimates for the rotation periods of  $23.07 \pm 0.16$  d for WASP-69 and  $14.36 \pm 0.35$  d for WASP-84. The WASP-69 data sets obtained in 2008 with both cameras 224 and 226 each show periods of  $\sim 23/2$  days, presumably as a result of multiple spot groups on the surface of the star during this observing season. The data on WASP-69 obtained by camera 223 in 2008 are affected by systematic instrumental noise and so are not useful for this analysis.

For both WASP-69 and WASP-84, we used a least-squares fit of the sinusoidal function and its first harmonic to model the rotational modulation in the lightcurves for each camera and season with rotation periods fixed at the best estimates. The results are shown in Figs. 6 and 7. We then subtracted this harmonic-series fit from the original WASP lightcurves prior to our analysis of the transit.

## 5 SYSTEM PARAMETERS FROM COMBINED ANALYSES

We determined the parameters of each system from a simultaneous fit to all photometric and radial-velocity data. The fit was performed using the current version of the Markov-chain Monte Carlo (MCMC) code described by Collier Cameron et al. (2007) and Pollacco et al. (2008).

The transit lightcurves are modelled using the formulation of Mandel & Agol (2002) with the assumption that the planet is much smaller than the star. Limb-darkening was accounted for using a four-coefficient, nonlinear limb-darkening model, using coefficients appropriate to the passbands from the tabulations of Claret (2000, 2004). The coefficients are interpolated once using the values of  $\log g_*$  and  $[\text{Fe}/\text{H}]$  of Table 5, but are interpolated at each MCMC step using the latest value of  $T_{\text{eff}}$ . The coefficient values corresponding to the best-fitting value of  $T_{\text{eff}}$  are given in Table 7. The transit lightcurve is parameterised by the epoch of mid-transit  $T_0$ , the orbital period  $P$ , the planet-to-star area ratio  $(R_p/R_*)^2$ , the approximate duration of the transit from initial to final contact  $T_{14}$ , and the impact parameter  $b = a \cos i/R_*$  (the distance, in fractional stellar radii, of the transit chord from the star's centre in the case of a circular orbit), where  $a$  is the semimajor axis and  $i$  is the inclination of the orbital plane with respect to the sky plane.

The eccentric Keplerian radial-velocity orbit is parameterised by the stellar reflex velocity semi-amplitude  $K_1$ , the systemic velocity  $\gamma$ , an instrumental offset between the HARPS and CORALIE spectrographs  $\Delta\gamma_{\text{HARPS}}$ , and  $\sqrt{e} \cos \omega$  and  $\sqrt{e} \sin \omega$  where  $e$  is orbital eccentricity and  $\omega$  is the argument of periastron. We use  $\sqrt{e} \cos \omega$  and  $\sqrt{e} \sin \omega$  as they impose a uniform prior on  $e$ , whereas the jump parameters we used previously,  $e \cos \omega$  and  $e \sin \omega$ , impose a linear prior that biases  $e$  toward higher values (Anderson et al. 2011).

The linear scale of the system depends on the orbital separation  $a$  which, through Kepler's third law, depends on the stellar mass  $M_*$ . At each step in the Markov chain, the latest values of  $\rho_*$ ,  $T_{\text{eff}}$  and  $[\text{Fe}/\text{H}]$  are input in to the empirical mass calibration of Enoch et al. (2010) (itself based on Torres, Andersen & Giménez 2010 and updated by Southworth 2011) to obtain  $M_*$ . The shapes of the transit lightcurves and the radial-velocity curve constrain stellar density  $\rho_*$  (Seager & Mallén-Ornelas 2003), which combines with  $M_*$  to give the stellar radius  $R_*$ . The stellar effective temperature

$T_{\text{eff}}$  and metallicity  $[\text{Fe}/\text{H}]$  are proposal parameters constrained by Gaussian priors with mean values and variances derived directly from the stellar spectra (see Section 3).

As the planet-to-star area ratio is determined from the measured transit depth, the planet radius  $R_p$  follows from  $R_*$ . The planet mass  $M_p$  is calculated from the the measured value of  $K_1$  and the value of  $M_*$ ; the planetary density  $\rho_p$  and surface gravity  $\log g_p$  then follow. We calculate the planetary equilibrium temperature  $T_{\text{eq}}$ , assuming zero albedo and efficient redistribution of heat from the planet's presumed permanent day side to its night side. We also calculate the durations of transit ingress ( $T_{12}$ ) and egress ( $T_{34}$ ).

At each step in the MCMC procedure, model transit lightcurves and radial velocity curves are computed from the proposal parameter values, which are perturbed from the previous values by a small, random amount. The  $\chi^2$  statistic is used to judge the goodness of fit of these models to the data and the decision as to whether to accept a step is made via the Metropolis-Hastings rule (Collier Cameron et al. 2007): a step is accepted if  $\chi^2$  is lower than for the previous step and a step with higher  $\chi^2$  is accepted with a probability proportional to  $\exp(-\Delta\chi^2/2)$ . This gives the procedure some robustness against local minima and results in a thorough exploration of the parameter space around the best-fitting solution.

For WASP-69 and WASP-84 we used WASP lightcurves detrended for rotational modulation (Section 4). We excluded the WASP-69 lightcurves from camera 223 as they suffer from greater scatter than the lightcurves from the other cameras. The WASP-70A lightcurves were corrected for dilution by WASP-70B using flux ratios derived from in-focus EulerCam and TRAPPIST images (Section 6). To give proper weighting to each photometry data set, the uncertainties were scaled at the start of the MCMC so as to obtain a photometric reduced- $\chi^2$  of unity.

For WASP-69b and WASP-70Ab the improvement in the fit to the RV data resulting from the use of an eccentric orbit model is small and is consistent with the underlying orbit being circular. We thus adopt circular orbits, which Anderson et al. (2012) suggest is the prudent choice for short-period,  $\sim$ Jupiter-mass planets in the absence of evidence to the contrary. In a far wider orbit, closer to that of the eccentric WASP-8b (Queloz et al. 2010), WASP-84b will experience weaker tidal forces and there is indication that the system is young (Section 8), so there is less reason to expect its orbit to be circular. Using the  $F$ -test approach of Lucy & Sweeney (1971), we calculate a 60 per cent probability that the improvement in the fit could have arisen by chance if the underlying orbit were circular, which is similar to the probabilities for the other two systems. There is very little difference between the circular solution and the eccentric solution: the stellar density and the inferred stellar and planetary dimensions differ by less than half a  $1\text{-}\sigma$  error bar. Thus we adopt a circular orbit for WASP-84b. We find  $2\text{-}\sigma$  upper limits on  $e$  of 0.10, 0.067 and 0.077 for, respectively, WASP-69b, -70Ab and -84b.

From initial MCMC runs we noted excess scatter in the RV residuals of both WASP-69 and WASP-84, with the residuals varying sinusoidally when phased on the stellar rotation periods, as derived from the WASP photometry (Figure 8). The RV residuals of WASP-69 are adequately fit by a sinusoid and those of WASP-84 benefit from the addition of the first harmonic:

$$RV_{\text{activity}} = a_1 \sin 2\pi\phi + b_1 \cos 2\pi\phi + a_2 \sin 4\pi\phi. \quad (1)$$

We phased the RV residuals of WASP-69, which were obtained over two seasons, with the average rotation period (23.07 d) derived from all available WASP photometry. For WASP-84 we chose to phase the RV residuals, which were obtained in a single season,

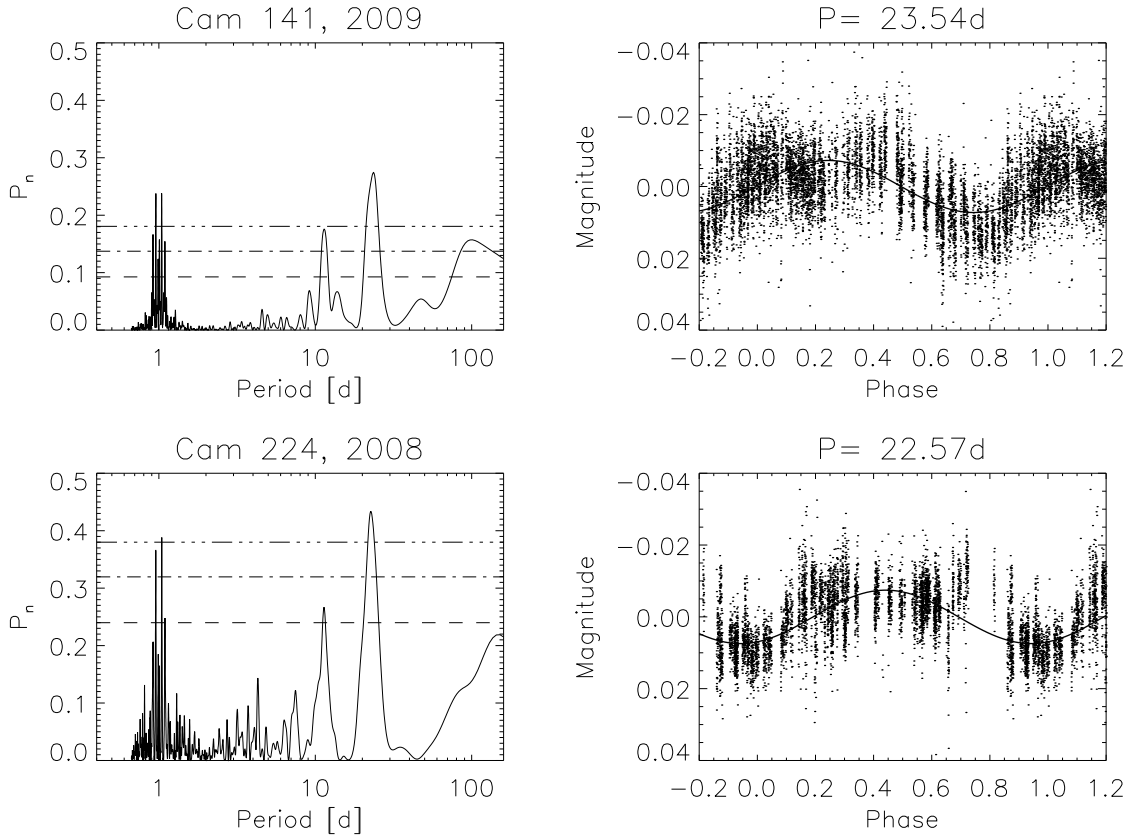


**Figure 4.** *Left panels:* Periodograms for the WASP data from two different observing seasons for WASP-69. Horizontal lines indicate false alarm probability levels  $FAP=0.1, 0.01, 0.001$ . The WASP camera and year of observation are noted in the titles; the first digit of the camera number denotes the observatory (1=SuperWASP-North and 2=WASP-South) and the third digit denotes the camera number. *Right panels* Lightcurves folded on the best periods as noted in the title.

**Table 6.** Frequency analysis of WASP lightcurves. Obs denotes WASP-South (S) or SuperWASP-North (N), Cam is the WASP camera number,  $N_{\text{points}}$  is the number of observations,  $P$  is the period of corresponding to the strongest peak in the periodogram, Amp is the amplitude of the best-fitting sine wave in mmag and FAP is the false-alarm probability.

| Year            | Obs                        | Cam | Baseline                | $N_{\text{points}}$ | $P/d$  | Amp | FAP                   |
|-----------------|----------------------------|-----|-------------------------|---------------------|--------|-----|-----------------------|
| <b>WASP-69:</b> |                            |     |                         |                     |        |     |                       |
| 2008            | S                          | 223 | 2008 Jun 04–Oct 12      | 6732                | 1.05   | 10  | $2.2 \times 10^{-2}$  |
| 2008            | S                          | 224 | 2008 Jun 04–Oct 12      | 6003                | 11.43  | 9   | $9.9 \times 10^{-4}$  |
| 2008            | N                          | 146 | 2008 Jun 26–Oct 08      | 2928                | 11.38  | 9   | $8.1 \times 10^{-4}$  |
| 2009            | S                          | 223 | 2009 May 19–Oct 11      | 4610                | 23.54  | 13  | $9.9 \times 10^{-3}$  |
| 2009            | S                          | 224 | 2009 May 19–Oct 11      | 5111                | 22.57  | 7   | $4.9 \times 10^{-4}$  |
| 2009            | N                          | 141 | 2009 Jun 26–Oct 08      | 6556                | 23.54  | 7   | $7.3 \times 10^{-5}$  |
| 2009            | N                          | 146 | 2009 Jun 26–Oct 08      | 6677                | 23.74  | 7   | $4.2 \times 10^{-6}$  |
| 2010            | N                          | 141 | 2010 Jun 26–Oct 06      | 6846                | 22.76  | 12  | $9.2 \times 10^{-10}$ |
| 2010            | N                          | 146 | 2010 Jun 26–Oct 06      | 6820                | 22.76  | 11  | $7.7 \times 10^{-6}$  |
| <b>WASP-70:</b> | No evidence of modulation. |     |                         |                     |        |     |                       |
| <b>WASP-84:</b> |                            |     |                         |                     |        |     |                       |
| 2009            | S                          | 226 | 2009 Jan 14–Apr 21      | 5161                | 13.450 | 10  | $2.1 \times 10^{-9}$  |
| 2010            | N                          | 143 | 2009 Dec 02–2010 Mar 31 | 3738                | 15.170 | 7   | $1.3 \times 10^{-4}$  |
| 2010            | S                          | 226 | 2010 Jan 15–Apr 21      | 4548                | 15.170 | 7   | $3.7 \times 10^{-6}$  |
| 2011            | N                          | 143 | 2010 Dec 02–2011 Mar 29 | 3701                | 14.000 | 15  | $1.8 \times 10^{-12}$ |
| 2011            | S                          | 226 | 2011 Jan 05–Mar 01      | 3684                | 14.000 | 14  | $1.4 \times 10^{-9}$  |

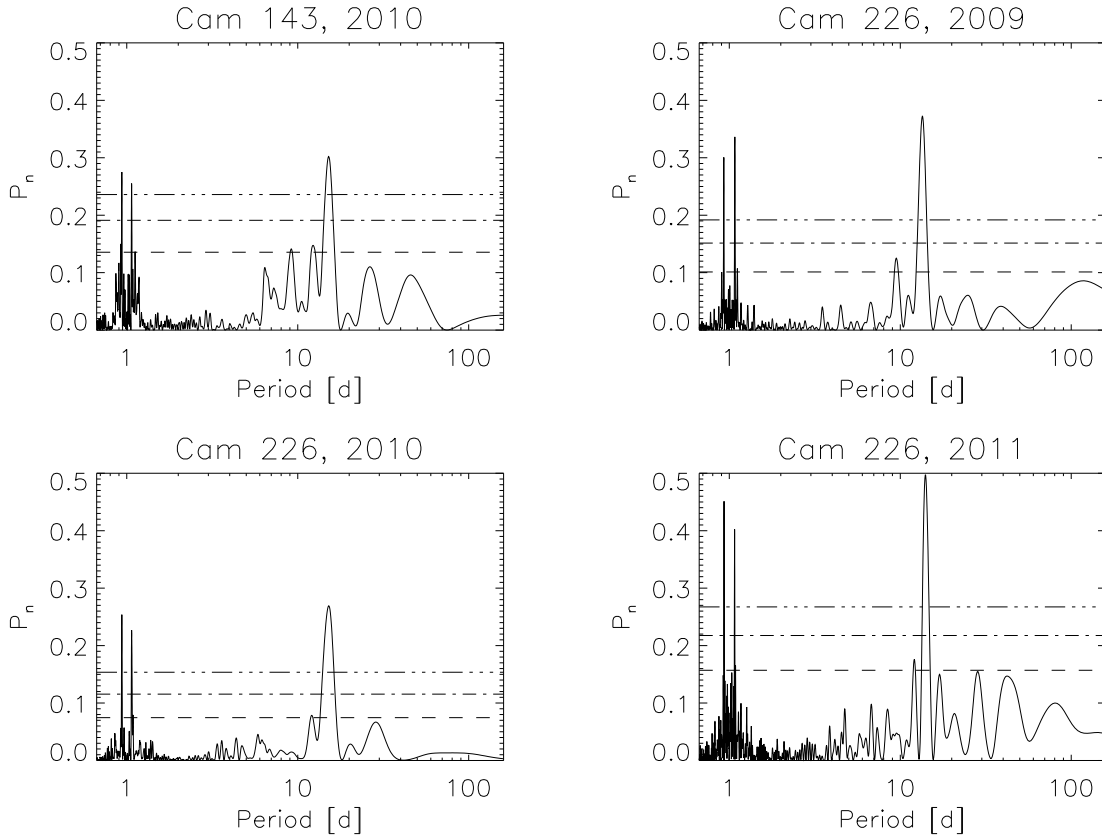


**Figure 5.** Periodograms of the WASP data for WASP-84 from four independent data sets. The WASP camera and year of observation are noted in the titles; the first digit of the camera number denotes the observatory (1=SuperWASP-North and 2=WASP-South) and the third digit denotes the camera number. Horizontal lines indicate false alarm probability levels  $FAP=0.1, 0.01, 0.001$ .

**Table 7.** Limb-darkening coefficients

| Star     | Imager          | Observation bands             | Claret band | $a_1$ | $a_2$  | $a_3$ | $a_4$  |
|----------|-----------------|-------------------------------|-------------|-------|--------|-------|--------|
| WASP-69  | WASP / EulerCam | Broad (400–700 nm) / Gunn $r$ | Cousins $R$ | 0.755 | -0.869 | 1.581 | -0.633 |
| WASP-69  | TRAPPIST        | Sloan $z'$                    | Sloan $z'$  | 0.824 | -0.922 | 1.362 | -0.549 |
| WASP-70A | WASP / EulerCam | Broad (400–700 nm) / Gunn $r$ | Cousins $R$ | 0.616 | -0.218 | 0.743 | -0.397 |
| WASP-70A | TRAPPIST        | Cousins $I$ + Sloan $z'$      | Sloan $z'$  | 0.690 | -0.484 | 0.828 | -0.402 |
| WASP-84  | WASP / RISE     | Broad (400–700 nm) / $V + R$  | Cousins $R$ | 0.695 | -0.591 | 1.269 | -0.589 |
| WASP-84  | TRAPPIST        | Sloan $z'$                    | Sloan $z'$  | 0.758 | -0.735 | 1.162 | -0.517 |

with the period derived from the photometry obtained in the preceding season (2011;  $P_{\text{rot}} = 14.0$  d), as we did not perform simultaneous monitoring. Pre-whitening the RVs using Equation 1 reduced the RMS of the residual scatter about the best-fitting Keplerian orbit from  $11.04 \text{ m s}^{-1}$  to  $8.28 \text{ m s}^{-1}$  in the case of WASP-69 and from  $14.81 \text{ m s}^{-1}$  to  $6.98 \text{ m s}^{-1}$  in the case of WASP-84 (Figure 8). The coefficients of the best-fitting activity models are given in Table 8.

A common alternative approach is to pre-whiten RVs using a relation derived from a linear fit between the RV residuals and the bisector spans, which are anticorrelated when stellar activity is the source of the signal (Melo et al. 2007). The WASP-69 RV residuals are essentially uncorrelated with the bisector spans ( $r = -0.14$ ) resulting in a small reduction in the RMS of the residual RVs, from  $11.04 \text{ m s}^{-1}$  to  $10.08 \text{ m s}^{-1}$  (see Figure 9). This is probably due to the star’s low  $v \sin I$  ( $2.2 \text{ km s}^{-1}$ ) as RV varies linearly

with  $v \sin I$ , but bisector span goes as  $(v \sin I)^{3.3}$  (Saar & Donahue 1997; Santos et al. 2003). The anticorrelation ( $r = -0.71$ ) between the RV residuals and the bisector spans of WASP-84 ( $v \sin I = 4.1 \text{ km s}^{-1}$ ) is strong and the RMS of the residual RVs is reduced from  $14.81 \text{ m s}^{-1}$  to  $11.08 \text{ m s}^{-1}$  (see Figure 9). The reduction in the scatter of the residual RVs obtained using this approach was less for both WASP-69 and WASP-84 than that obtained using the harmonic-fitting approach; we thus elected to use the RVs pre-whitened by subtracting harmonic functions in the MCMC analyses.

For both WASP-69 and WASP-84 the best-fitting solution is essentially unchanged by the pre-whitening. One parameter that we could expect to be affected, via a modified  $K_1$ , is the planetary mass. For WASP-69b we obtain  $M_P = 0.260 \pm 0.017 M_{\text{Jup}}$  when using pre-whitened RVs and  $M_P = 0.253 \pm 0.022 M_{\text{Jup}}$  otherwise.

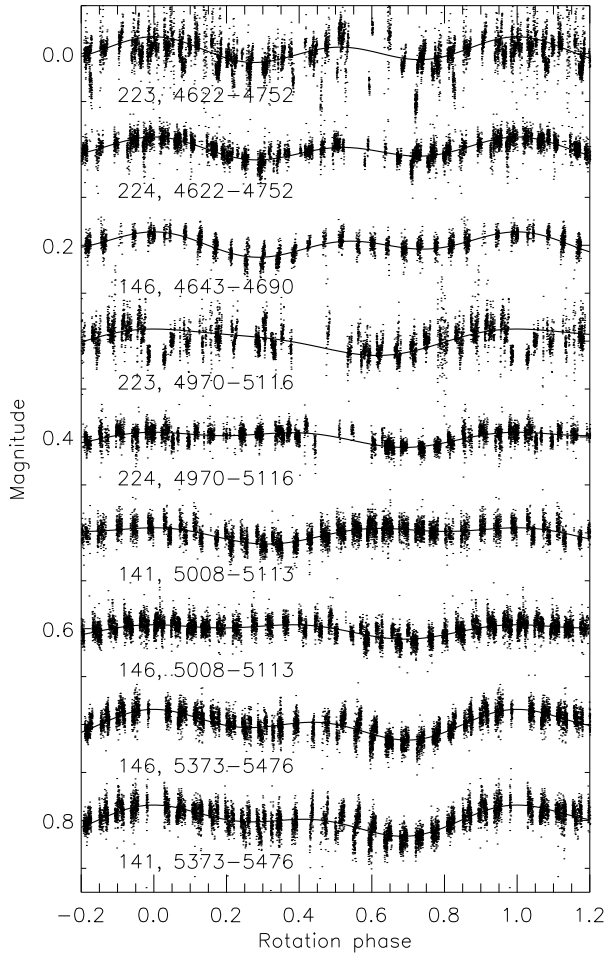


**Figure 6.** WASP lightcurves of WASP-69 plotted as a function of rotation phase for  $P_{\text{rot}} = 23.07$  d. The data, detrended by SYSREM, for each combination of observing season and camera are offset by multiples of 0.1 magnitudes. Each lightcurve is labelled with its camera number and the date range it spans, in truncated Julian Date: JD - 2450 000. Solid lines show the harmonic fit used to remove the rotational modulation prior to modeling the transit.

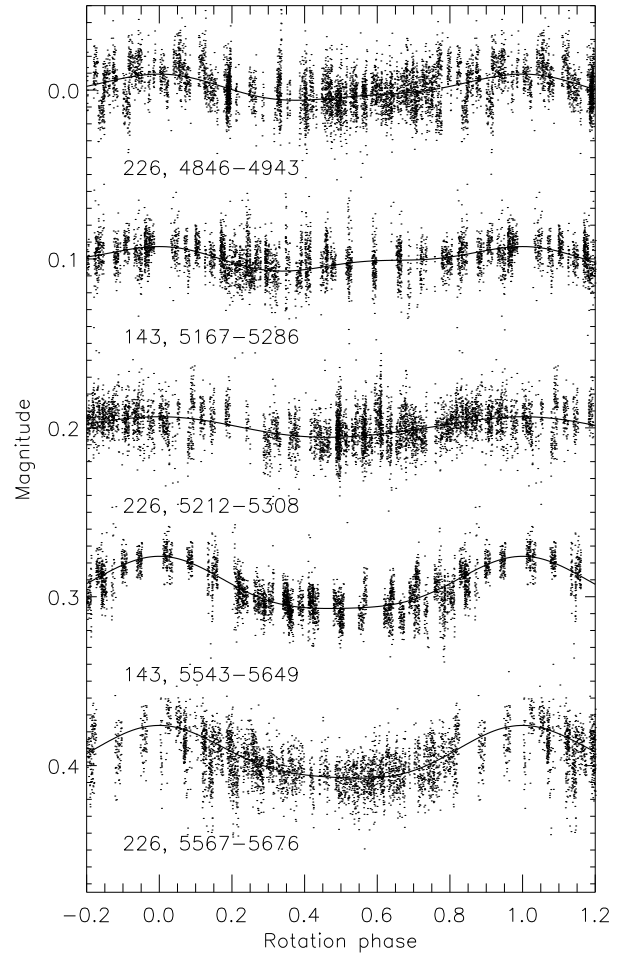


**Figure 7.** WASP lightcurves of WASP-84 plotted as a function of rotation phase for  $P_{\text{rot}} = 14.36$  d. Caption as for Fig 6.

**Table 8.** Coefficients of the activity-induced RV variations model

| Star    | $a_1$<br>( $\text{m s}^{-1}$ ) | $b_1$<br>( $\text{m s}^{-1}$ ) | $a_2$<br>( $\text{m s}^{-1}$ ) |
|---------|--------------------------------|--------------------------------|--------------------------------|
| WASP-69 | $8.8 \pm 2.6$                  | $4.5 \pm 2.7$                  | 0                              |
| WASP-84 | $12.1 \pm 2.3$                 | $-6.5 \pm 2.8$                 | $-10.9 \pm 2.5$                |

For WASP-84b we obtain  $M_p = 0.694 \pm 0.028 M_{\text{Jup}}$  when using pre-whitened RVs and  $M_p = 0.691_{-0.032}^{+0.061} M_{\text{Jup}}$  otherwise.

To obtain a spectroscopic reduced  $\chi^2$  of unity we added a ‘jitter’ term in quadrature to the formal RV errors. Pre-whitening reduced the jitter required from  $10.1 \text{ m s}^{-1}$  to  $6.7 \text{ m s}^{-1}$  for WASP-69 and from  $13.5 \text{ m s}^{-1}$  to zero for WASP-84; the jitter for WASP-70A was  $3.9 \text{ m s}^{-1}$ . We excluded two in-transit WASP-70A RVs from the analysis as we did not model the Rossiter-McLaughlin effect (e.g. Brown et al. 2012).

We explored the possible impact of spots on our determination of the system parameters of WASP-69 and WASP-84. We assumed that the stars’ visible faces were made permanently dimmer, by spots located outside of the transit chords, at the level of the maximum amplitudes of the rotational-modulation signals found from the WASP photometry (Table 6). Having corrected the transit lightcurves for this, we performed MCMC analyses again and found the stellar and planetary dimensions (density, radius, mass) to have changed by less than  $0.2 \sigma$ .

The system parameters from the combined analyses are given in Table 9 and the best fits to the radial velocities and the photometry are plotted in Figures 1, 2 and 3.

## 6 THE WASP-69 SYSTEM

WASP-69b is a bloated Saturn-mass planet ( $0.26 M_{\text{Jup}}$ ,  $1.06 R_{\text{Jup}}$ ) in a 3.868-d orbit around an active mid-K dwarf. The system is expected to be a favourable target for transmission spectroscopy owing to the large predicted scale height of the planet’s atmosphere and the apparent brightness and the small size of the star. The parameters derived from the spectral analysis and the MCMC analysis are given, respectively, in Tables 5 and 9 and the corresponding transit and Keplerian orbit models are superimposed, respectively, on the radial velocities and the photometry in Figure 1.

We estimated the stellar rotation period  $P_{\text{rot}}$  from activity-rotation induced modulation of the WASP lightcurves to be  $23.07 \pm 0.16 \text{ d}$ . Together with our estimate of the stellar radius (Table 9), this implies a rotation speed of  $v = 1.78 \pm 0.06 \text{ km s}^{-1}$ , which can be compared with the spectroscopic estimate of the projected rotation speed of  $v \sin I = 2.2 \pm 0.4 \text{ km s}^{-1}$ .

The rotation rate ( $P \leq 18.7 \pm 3.5 \text{ d}$ ) implied by the  $v \sin I$  gives a gyrochronological age of  $0.73 \pm 0.28 \text{ Gyr}$  using the Barnes (2007) relation. The lightcurve-modulation period implies a slightly older gyrochronological age of  $1.10 \pm 0.15 \text{ Gyr}$ .

There is no significant detection of lithium in the spectra of WASP-69, with an equivalent-width upper limit of 12 m, corresponding to an abundance upper limit of  $\log A(\text{Li}) < 0.05 \pm 0.07$ . This implies an age of at least 0.5 Gyr (Sestito & Randich 2005).

There are strong emission peaks evident in the Ca II H+K lines (Figure 10), with an estimated activity index of  $\log R'_{\text{HK}} \sim -4.54$ . This gives an approximate age of  $\sim 0.8 \text{ Gyr}$  according to Mamajek & Hillenbrand (2008), which is consistent with the age implied from the rotation rate and the absence of lithium.

Interestingly, the observed rotation period and the 2MASS  $J -$

$K$  value of 0.57 suggest an age closer to 3 Gyr if we apply  $P \approx \sqrt{t}$  using the Coma Berenices cluster colour-rotation distribution as a benchmark (Collier Cameron et al. 2009). This is consistent with the lack of lithium, but slightly at odds with the  $\log R'_{\text{HK}}$  and the Barnes (2007) gyrochronological ages.

As a low-density planet in a short orbit around a relatively-young, active star, WASP-69b could be undergoing significant mass loss due to X-ray-driven or extreme-ultraviolet-driven evaporation (e.g. Lecavelier Des Etangs 2007; Jackson, Davis & Wheatley 2012). At earlier times the stellar X-ray luminosity, and hence the planetary mass loss rate, would have been higher. ROSAT recorded an X-ray source 1RXS J210010.1–050527 with a count rate of  $2.4 \pm 0.9 \text{ s}^{-1}$  over 0.1–2.4 keV and at an angular distance of  $60 \pm 27''$  from WASP-69. There is no optical source spatially coincident with the ROSAT source position. The brightest object in the NOMAD catalog located within  $60''$  of the ROSAT source is  $30''$  away and has  $R=16.6$ , whereas WASP-69 is at  $60''$  and has  $R=9.2$ . Assuming a uniform sky distribution for the 18 811 bright sources (count rate  $> 0.05 \text{ s}^{-1}$ ) of the ROSAT all-sky catalogue (Voges et al. 1999), the probability that an unrelated source is within  $120''$  of WASP-69 is 0.05 per cent.

Thus, assuming the ROSAT source to be WASP-69, we follow Jackson, Davis & Wheatley (2012) to estimate a current planetary mass loss rate of  $10^{12} \text{ g s}^{-1}$ , having assumed an evaporation efficiency factor of 0.25 and having converted the count rate to an X-ray luminosity ( $\log(L_X/L_{\text{bol}}) = -4.43$ ; Fleming, Schmitt & Giampapa 1995). This can be compared with the mass-loss rates of HD 209458b and HD 189733b, estimated at  $\sim 10^{10-11} \text{ g s}^{-1}$  from observations of Lyman  $\alpha$  absorption by escaping hydrogen atoms (Vidal-Madjar et al. 2003; Lecavelier Des Etangs et al. 2010). Jackson, Davis & Wheatley (2012) estimate that a star of similar spectral type as WASP-69 has a saturated X-ray luminosity ratio of  $\log(L_X/L_{\text{bol}})_{\text{sat}} \sim -3.35$  for the first  $\sim 200 \text{ Myr}$  of its life. Assuming WASP-69b to have been in-situ during this period suggests the planet would have lost mass at a rate of  $\sim 10^{13} \text{ g s}^{-1}$  and, assuming a constant planetary density, the planet to have undergone a fractional mass loss of  $\sim 0.2$ .

## 7 THE WASP-70 SYSTEM

WASP-70Ab is a  $0.59 M_{\text{Jup}}$  planet in a 3.713-d orbit around the primary of a spatially-resolved G4+K3 binary. The parameters derived from the spectral analysis and the MCMC analysis are given, respectively, in Tables 5 and 9 and the corresponding transit and Keplerian orbit models are superimposed, respectively, on the radial velocities and the photometry in Figure 2.

2MASS images reveal that the two stars are separated by  $\sim 3''$  with a position angle of  $167^\circ$ . We obtained in-focus TRAPPIST  $I + z'$  and EulerCam Gunn  $r$  images in 2011 and 2012, respectively (Figure 11). These show the two stars separated by  $3''.3$  at a position angle of  $167^\circ$ , which is consistent with no significant relative motion since the 2MASS images were taken in 1998. The projected separation of  $3''.3$  and inferred distance of 245 pc, give a physical separation of the two stars of at least 800 AU. Further evidence of the stars’ association comes from the mean radial velocities measured from CORALIE spectra:  $-65.4 \text{ km s}^{-1}$  and  $-64.6 \text{ km s}^{-1}$  for WASP-70A and WASP-70B, respectively.

We determined the flux ratios of the stellar pair from aperture photometry of the images. For the EulerCam images, we used the USNO-B1.0 magnitudes of comparison stars to determine approximate  $r$ -band magnitudes (Table 10). By combining these with

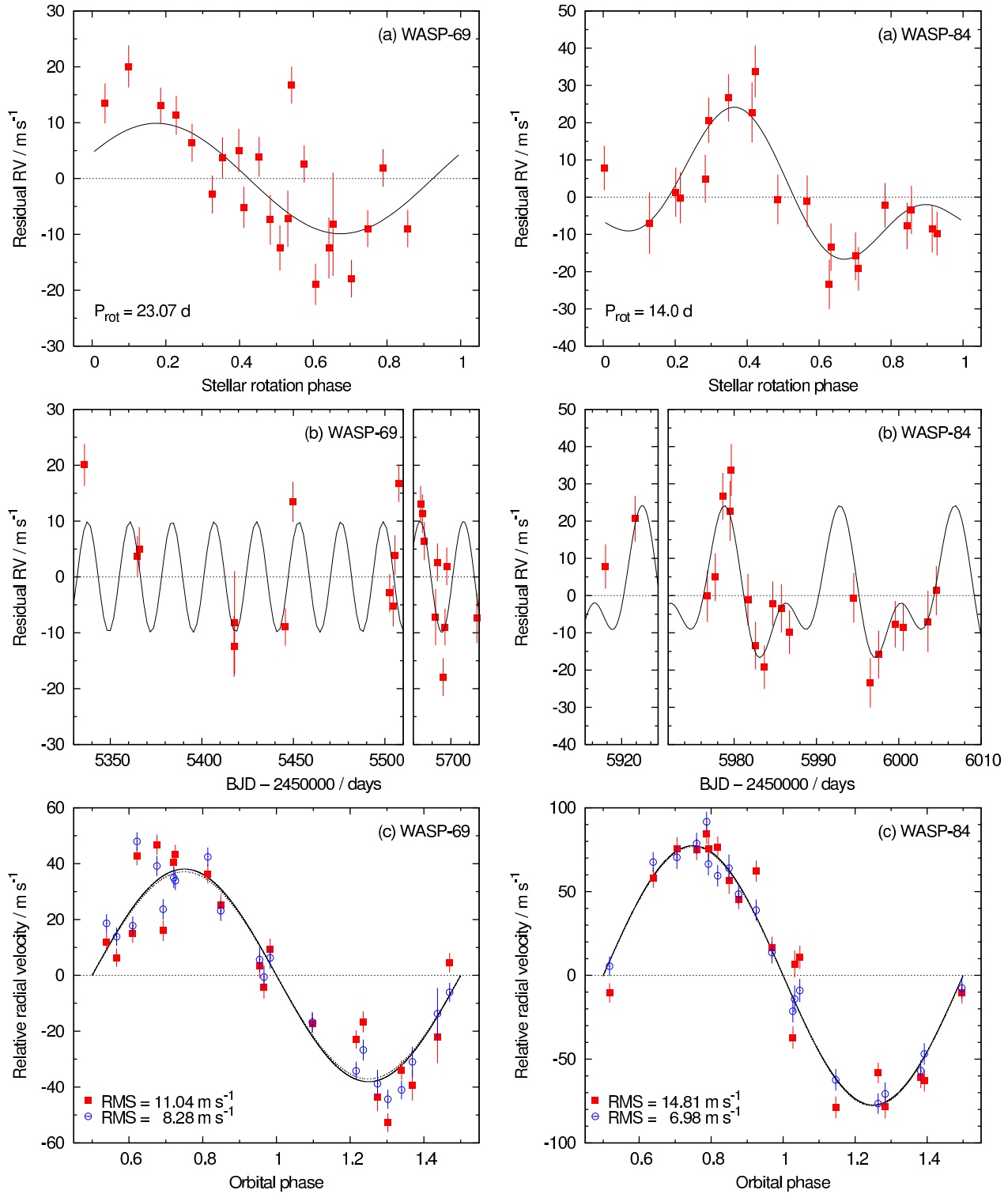


**Figure 8.** The radial-velocity modulation induced by stellar activity. The panels on the left pertain to WASP-69 and those on the right pertain to WASP-84; the remainder of the caption describes the plots of both stars. **(a)** The residuals about the best-fitting Keplerian orbit phased on a period derived from a modulation analysis of the WASP photometry. The best-fitting harmonic function is overplotted (see Equation 1 and Table 8). **(b)** The residuals about the best-fitting Keplerian orbit as a function of time; the best-fitting harmonic function is overplotted. The abscissa scales on the two adjacent panels are equal. Specific to WASP-69, two points are not plotted; one was taken a season earlier and the other a season later than the data shown. With reference to the top-left panel (panel (a) for WASP-69), the ‘early’ point is at coordinate (0.61, -19) and the ‘late’ point is at coordinate (0.51, -12). **(c)** The RVs, both detrended and non-detrended, folded on the transit ephemeris. By first detrending the RVs with the harmonic function a significantly lower scatter is obtained (the blue circles about the dashed line) as compared to the non-detrended RVs (the red squares about the solid line).

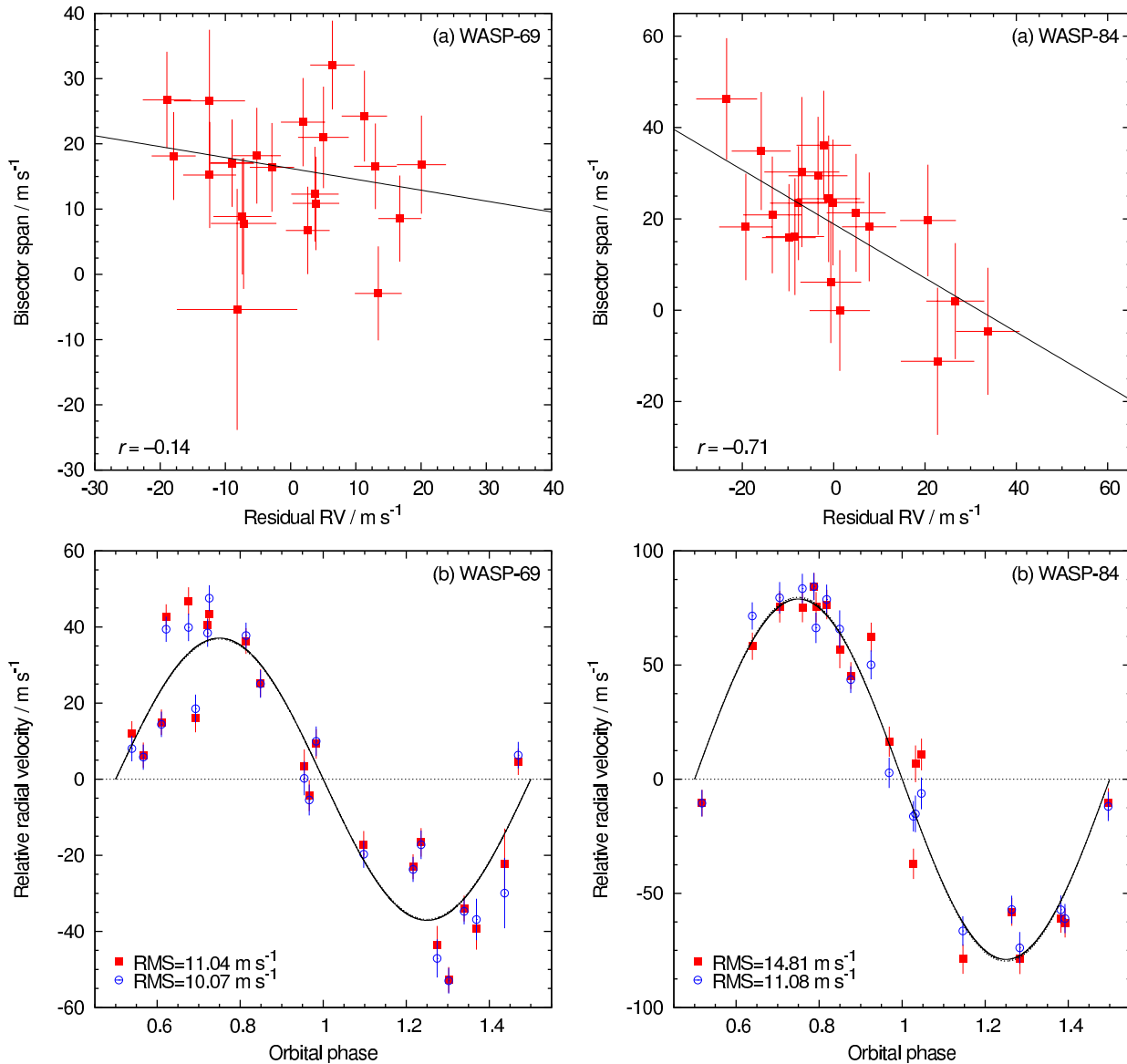


**Figure 9.** The anticorrelated variations in bisector span and radial velocity induced by stellar activity. From initial MCMCs for both WASP-69 and WASP-84, we noted large scatter about the best-fitting Keplerian orbits, which we suggest to be the product of stellar activity. The panels on the left pertain to WASP-69 and those on the right pertain to WASP-84; the remainder of the caption describes the plots of both stars. **(a):** Similar to Melo et al. (2007), we found the residuals to be anticorrelated with bisector span. A linear fit to the data is overplotted and the correlation coefficient,  $r$  is given. **(b):** By first detrending the RVs with this bisector-residual relation, a smaller scatter about the best-fitting Keplerian orbit is obtained (the blue circles about the dashed line) as compared to the non-detrended RVs (the red squares about the solid line). The result is inferior to that obtained when detrending the RVs with low-order harmonic series (Figure 8).

the  $T_{\text{eff}}$  from the spectral analysis we constructed a Hertzsprung-Russell diagram for the WASP-70 double system (Figure 12). A distance modulus of  $6.95 \pm 0.15$  ( $\equiv 245 \pm 20$  pc) was required to bring the companion star on to the main sequence. WASP-70A appears to have evolved off the ZAMS with an age of around 9–10 Gyr.

The rotation rate for WASP-70A ( $P \leq 34.1 \pm 7.8$  d) implied by the  $v \sin I$  gives a gyrochronological age of  $\leq 7 \pm 3$  Gyr using the Barnes (2007) relation. There is no significant detection of lithium in the spectra, with equivalent-width upper limits of 11m and 20m, corresponding to abundance upper limits of  $\log A(\text{Li}) < 1.20 \pm 0.07$  and  $< 0.71 \pm 0.25$  for WASP-70A and B, respectively. These imply

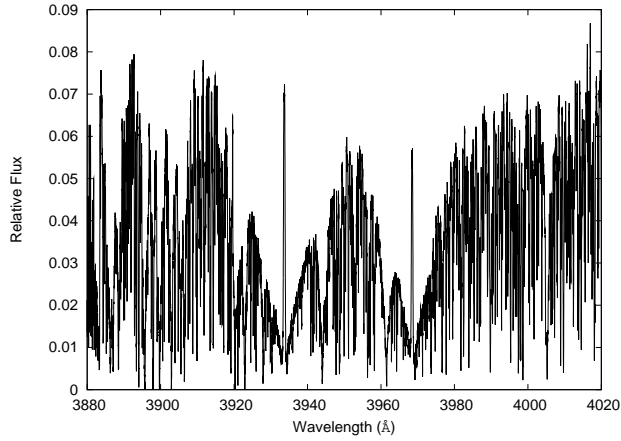
an age of at least  $\sim 5$  Gyr (Sestito & Randich 2005) for WASP-70A and over 600 Myr for WASP-70B. We found no evidence of modulation in the WASP-70A+B lightcurves or of emission peaks in the Ca II H+K lines in either star.

## 8 THE WASP-84 SYSTEM

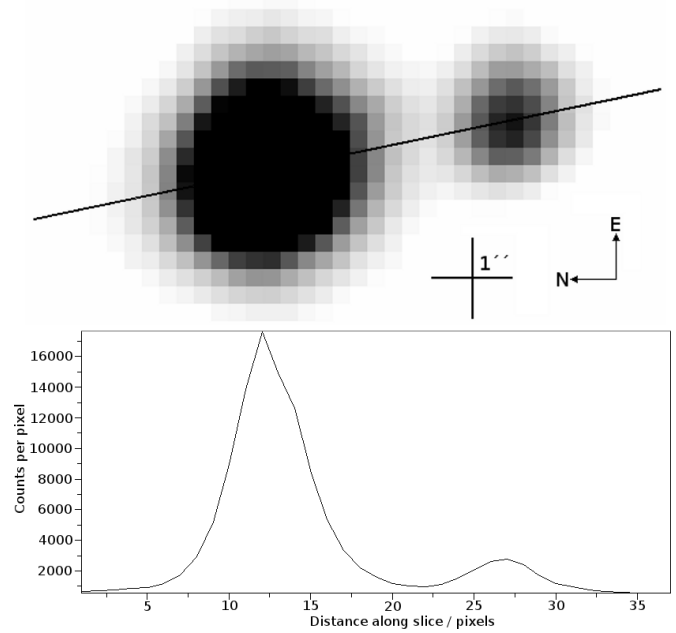
WASP-84b is a  $0.69-M_{\text{Jup}}$  planet in an 8.523-d orbit around an early-K dwarf. After HAT-P-15b and HAT-P-17b, which have orbital periods of 10.86 d and 10.34 d, respectively, WASP-84b has the longest orbital period of the planets discovered from the ground by the transit technique (Kovács et al. 2010; Howard et al. 2012).

**Table 9.** System parameters

| Parameter                              | Symbol (Unit)                                       | WASP-69b                             | WASP-70Ab                             | WASP-84b                              |
|--|---|--------------------------------------|---------------------------------------|---------------------------------------|
| Orbital period                         | $P$ (d)   | $3.8681382 \pm 0.0000017$            | $3.7130203 \pm 0.0000047$             | $8.5234865 \pm 0.0000070$             |
| Epoch of mid-transit                   | $T_c$ (BJD, UTC)                                    | $2455748.83344 \pm 0.00018$          | $2455736.50348 \pm 0.00027$           | $2456286.10583 \pm 0.00009$           |
| Transit duration                       | $T_{14}$ (d)  | $0.0929 \pm 0.0012$                  | $0.1389^{+0.0014}_{-0.0019}$          | $0.11452 \pm 0.00046$                 |
| Transit ingress/egress duration        | $T_{12} = T_{34}$ (d)                               | $0.0192 \pm 0.0014$                  | $0.0150^{+0.0021}_{-0.0016}$          | $0.02064 \pm 0.00060$                 |
| Planet-to-star area ratio              | $\Delta F = R_p^2/R_*^2$                            | $0.01786 \pm 0.00042$                | $0.00970^{+0.00022}_{-0.00026}$       | $0.01678 \pm 0.00015$                 |
| Impact parameter                       | $b$   | $0.686 \pm 0.023$                    | $0.431^{+0.076}_{-0.169}$             | $0.632 \pm 0.012$                     |
| Orbital inclination                    | $i$ ( $^\circ$ )                                    | $86.71 \pm 0.20$                     | $87.12^{+1.24}_{-0.65}$               | $88.368 \pm 0.050$                    |
| Stellar reflex velocity semi-amplitude | $K_1$ ( $\text{m s}^{-1}$ )                         | $38.1 \pm 2.4$                       | $72.3 \pm 2.0$                        | $77.4 \pm 2.0$                        |
| Systemic velocity                      | $\gamma$ ( $\text{m s}^{-1}$ )                      | $-9628.26 \pm 0.23$                  | $-65389.74 \pm 0.32$                  | $-11578.14 \pm 0.33$                  |
| Offset between CORALIE and HARPS       | $\Delta\gamma_{\text{HARPS}}$ ( $\text{m s}^{-1}$ ) | —                                    | $15.44 \pm 0.11$                      | —                                     |
| Eccentricity                           | $e$   | 0 (adopted) ( $<0.10$ at $2\sigma$ ) | 0 (adopted) ( $<0.067$ at $2\sigma$ ) | 0 (adopted) ( $<0.077$ at $2\sigma$ ) |
| Stellar mass                           | $M_*$ ( $M_\odot$ )                                 | $0.826 \pm 0.029$                    | $1.106 \pm 0.042$                     | $0.842 \pm 0.037$                     |
| Stellar radius                         | $R_*$ ( $R_\odot$ )                                 | $0.813 \pm 0.028$                    | $1.215^{+0.064}_{-0.089}$             | $0.748 \pm 0.015$                     |
| Stellar surface gravity                | $\log g_*$ (cgs)                                    | $4.535 \pm 0.023$                    | $4.314^{+0.052}_{-0.036}$             | $4.616 \pm 0.011$                     |
| Stellar density                        | $\rho_*$ ( $\rho_\odot$ )                           | $1.54 \pm 0.13$                      | $0.619^{+0.136}_{-0.077}$             | $2.015 \pm 0.070$                     |
| Stellar effective temperature          | $T_{\text{eff}}$ (K)                                | $4715 \pm 50$                        | $5763 \pm 79$                         | $5314 \pm 88$                         |
| Stellar metallicity                    | [Fe/H]  | $0.144 \pm 0.077$                    | $-0.006 \pm 0.063$                    | $0.00 \pm 0.10$                       |
| Planetary mass                         | $M_p$ ( $M_{\text{Jup}}$ )                          | $0.260 \pm 0.017$                    | $0.590 \pm 0.022$                     | $0.694 \pm 0.028$                     |
| Planetary radius                       | $R_p$ ( $R_{\text{Jup}}$ )                          | $1.057 \pm 0.047$                    | $1.164^{+0.073}_{-0.102}$             | $0.942 \pm 0.022$                     |
| Planetary surface gravity              | $\log g_p$ (cgs)                                    | $2.726 \pm 0.046$                    | $3.000^{+0.066}_{-0.050}$             | $3.253 \pm 0.018$                     |
| Planetary density                      | $\rho_p$ ( $\rho_j$ )                               | $0.219 \pm 0.031$                    | $0.375^{+0.104}_{-0.060}$             | $0.830 \pm 0.048$                     |
| Orbital major semi-axis                | $a$ (AU)  | $0.04525 \pm 0.00053$                | $0.04853 \pm 0.00062$                 | $0.0771 \pm 0.0012$                   |
| Planetary equilibrium temperature      | $T_{\text{eq}}$ (K)                                 | $963 \pm 18$                         | $1387 \pm 40$                         | $797 \pm 16$                          |

**Figure 10.** CORALIE spectrum of WASP-69 showing strong emission in the Ca II H+K line cores.**Table 10.** Estimated magnitudes and flux ratios of WASP-70A+B

| Band     | WASP-70A | WASP-70B | $\Delta_{A-B}$ | $f_B/f_A$ |
|----------|----------|----------|----------------|-----------|
| $r$      | 10.8     | 13.1     | -2.3           | 0.12      |
| $I + z'$ | ...      | ...      | -1.6           | 0.22      |

**Figure 11.** Upper portion: EulerCam Gunn- $r$  image of WASP-70A+B; the B component is at a distance of  $3''.3$  and position angle of  $167^\circ$ . Lower portion: The counts per pixel along the slice marked on the image.

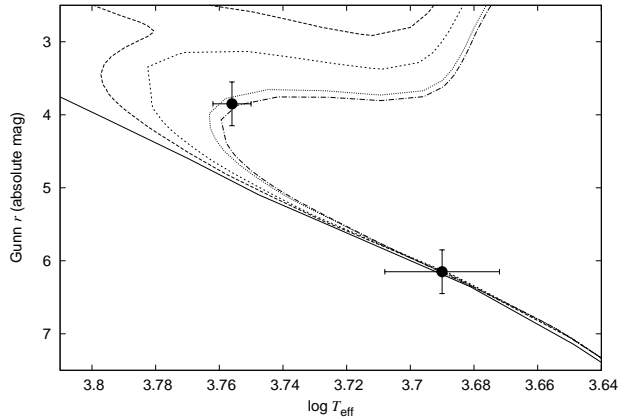


**Figure 12.** H-R diagram for WASP-70A+B. Various isochrones from Marigo et al. (2008) are plotted, with ages of 0, 3, 5, 9 and 10 Gyr.

The parameters derived from the spectral analysis and the MCMC analysis are given, respectively, in Tables 5 and 9 and the corresponding transit and Keplerian orbit models are superimposed, respectively, on the radial velocities and the photometry in Figure 3.

We estimated the stellar rotation period from the modulation of the WASP lightcurves to be  $P_{\text{rot}} = 14.36 \pm 0.35$  d. Together with our estimates of the stellar radius (Table 9), this implies a rotation speed of  $v = 2.64 \pm 0.08$  km s<sup>-1</sup>. This is inconsistent with the spectroscopic estimate of the projected rotation speed of  $v \sin I = 4.1 \pm 0.3$  km s<sup>-1</sup>. This disagreement may be due to an overestimation of  $v \sin I$  and an underestimation of  $R_*$ . We took macroturbulence values from the tabulation of Bruntt et al. (2010a). If we instead adopted a higher macroturbulence value from Gray (2008) then we would obtain a lower  $v \sin I$  of  $\sim 3.5$  km s<sup>-1</sup>. Similarly, systematics in the lightcurves or a limitation of the empirical mass calibration could have resulted in an underestimation of the stellar radius.

Using the Barnes (2007) relation,  $P_{\text{rot}}$  gives a gyrochronological age of  $0.79 \pm 0.12$  Gyr, whereas the rotation rate implied by the  $v \sin I$  ( $P \leq 9.2 \pm 0.7$  d) gives  $\leq 0.34 \pm 0.07$  Gyr.

There is no significant detection of lithium in the spectra, with an equivalent width upper limit of 8m, corresponding to an abundance upper limit of  $\log A(\text{Li}) < 0.12 \pm 0.11$ . This implies an age of at least  $\sim 0.5$  Gyr (Sestito & Randich 2005).

There are emission peaks evident in the Ca II H+K lines, with an estimated activity index of  $\log R'_{\text{HK}} \sim -4.43$ . This gives an approximate age of 0.4 Gyr according to Mamajek & Hillenbrand (2008).

Using the Coma Berenices cluster colour-rotation relation of Collier Cameron et al. (2009) we find an age of 1.4 Gyr. As was the case with WASP-69, this is at odds with the  $\log R'_{\text{HK}}$  and the Barnes (2007) gyrochronological ages.

## 9 DISCUSSION AND SUMMARY

We reported the discovery of the transiting exoplanets WASP-69b, WASP-70Ab and WASP-84b, each of which orbits a bright star ( $V \sim 10$ ). We derived the system parameters from a joint analysis of the WASP survey photometry, the CORALIE and HARPS radial velocities and the high-precision photometry from TRAPPIST, EulerCam and RISE.

WASP-69b is a bloated Saturn-type planet ( $0.26 M_{\text{Jup}}$ ,

$1.06 R_{\text{Jup}}$ ) in a 3.868-d period around a mid-K dwarf. We find WASP-69 to be active from emission peaks in the Ca II H+K lines ( $\log R'_{\text{HK}} \sim -4.54$ ) and from modulation of the star's lightcurves ( $P_{\text{rot}} = 23.07 \pm 0.16$  d; amplitude = 7–13 mmag). Both the gyrochronological calibration of Barnes (2007) and the age-activity relation of Mamajek & Hillenbrand (2008) suggest an age of around 1 Gyr, whereas the Coma Berenices colour-rotation calibration of (Collier Cameron et al. 2009) suggests an age closer to 3 Gyr.

WASP-70Ab is a Jupiter-type planet ( $0.59 M_{\text{Jup}}$ ,  $1.16 R_{\text{Jup}}$ ) in a 3.713-d orbit around the primary of a spatially-resolved G4+K3 binary separated by  $3''.3$  ( $\geq 800$  AU). An absence of emission in the Ca II H+K lines and an absence of lightcurve modulation indicates WASP-70A is relatively inactive. We used the binary nature of the system to construct an H-R diagram, from which we estimate its age to be 9–10 Gyr.

WASP-84b is a Jupiter-type planet ( $0.69 M_{\text{Jup}}$ ,  $0.94 R_{\text{Jup}}$ ) in an 8.523-d orbit around an active early-K dwarf. The planet has the third-longest period of the transiting planets discovered from the ground. We find WASP-84 to be active from emission peaks in the Ca II H+K lines ( $\log R'_{\text{HK}} \sim -4.43$ ) and from modulation of the star's lightcurves ( $P = 14.36 \pm 0.35$  d; amplitude = 7–15 mmag). The gyrochronological calibration of Barnes (2007) suggests an age of  $\sim 0.8$  Gyr for WASP-84, whereas the age-activity relation of Mamajek & Hillenbrand (2008) suggests an age of  $\sim 0.4$  Gyr.

We used the empirical relations of Enoch, Collier Cameron & Horne (2012), derived from fits to the properties of a well-characterised sample of transiting planets, to predict the radii of the three presented planets. The difference between the observed radii (Table 9) and the predicted radii of both WASP-70Ab ( $\Delta R_{\text{p,obs-pred}} = -0.067 R_{\text{Jup}}$ ) and WASP-84b ( $\Delta R_{\text{p,obs-pred}} = 0.065 R_{\text{Jup}}$ ) are small. For comparison, the average difference between the predicted and observed radii for the sample of Enoch, Collier Cameron & Horne (2012) is  $0.11 R_{\text{Jup}}$ . The predicted radius of WASP-69b ( $0.791 R_{\text{Jup}}$ ) is smaller than the observed radius (Table 9) by  $0.266 R_{\text{Jup}}$ , showing the planet to be bloated.

We observed excess scatter in the radial-velocity (RV) residuals about the best-fitting Keplerian orbits for the two active stars WASP-69 and WASP-84. Phasing the RV residuals on the photometrically-determined stellar rotation periods showed the excess scatter to be induced by a combination of stellar activity and rotation. We fit the residuals with low-order harmonic series and subtracted the best fits from the RVs prior to deriving the systems' parameters. The systems' solutions were essentially unchanged by this, with much less than a  $1\text{-}\sigma$  change to the planet mass in each case. We found this method of pre-whitening using a harmonic fit to result in a greater reduction in the residual RV scatter ( $\Delta\text{RMS} = -2.76$  m s<sup>-1</sup> for WASP-69 and  $\Delta\text{RMS} = -7.83$  m s<sup>-1</sup> for WASP-84) than the more traditional method of pre-whitening with a fit to the RV residuals and the bisector spans ( $\Delta\text{RMS} = -0.96$  m s<sup>-1</sup> for WASP-69 and  $\Delta\text{RMS} = -3.73$  m s<sup>-1</sup> for WASP-84). The poor performance of the bisector-RV fit method for WASP-69 probably stems from the slow rotation of the star, which has been shown to limit the method's efficacy (Saar & Donahue 1997; Santos et al. 2003).

WASP-69 and WASP-84 are two of the most active stars known to host exoplanets. Of the 303 systems with measured  $\log R'_{\text{HK}}$  values only 17 are more active than WASP-69 and only

6 are more active than WASP-84<sup>1</sup>. Conversely, only 14 exoplanet host stars have measured  $\log R'_{\text{HK}}$  indices indicating lower activity levels than WASP-70A, though values for inactive stars are probably underreported.

## ACKNOWLEDGEMENTS

WASP-South is hosted by the South African Astronomical Observatory and SuperWASP-North is hosted by the Isaac Newton Group on La Palma. We are grateful for their ongoing support and assistance. Funding for WASP comes from consortium universities and from the UK's Science and Technology Facilities Council. TRAPPIST is funded by the Belgian Fund for Scientific Research (Fond National de la Recherche Scientifique, FNRS) under the grant FRFC 2.5.594.09.F, with the participation of the Swiss National Science Foundation (SNF). The Liverpool Telescope is operated on the island of La Palma by Liverpool John Moores University in the Spanish Observatorio del Roque de los Muchachos of the Instituto de Astrofísica de Canarias with financial support from the UK Science and Technology Facilities Council. M. Gillon and E. Jehin are FNRS Research Associates. A. H.M.J. Triaud is a Swiss National Science Foundation fellow under grant number PBGEP2-145594. L. Delrez is a FNRS/FRIA Doctoral Fellow. We are grateful to R. D. Jeffries for discussion of the ROSAT catalog. This research has made use of the Exoplanet Orbit Database and the Exoplanet Data Explorer at <http://exoplanets.org> and the VizieR catalogue access tool, CDS, Strasbourg, France. The original description of the VizieR service was published in *A&AS* 143, 23.

## REFERENCES

- Anderson D. R. et al., 2012, *MNRAS*, 422, 1988  
 —, 2011, *ApJ*, 726, L19  
 Angerhausen D., Krabbe A., 2011, in *Astronomical Society of the Pacific Conference Series*, Vol. 450, *Astronomical Society of the Pacific Conference Series*, Beaulieu J. P., Dieters S., Tinetti G., eds., p. 55  
 Bakos G., Noyes R. W., Kovács G., Stanek K. Z., Sasselov D. D., Domsa I., 2004, *PASP*, 116, 266  
 Bakos G. Á. et al., 2013, *PASP*, 125, 154  
 Baranne A. et al., 1996, *A&AS*, 119, 373  
 Barnes S. A., 2007, *ApJ*, 669, 1167  
 Brown D. J. A. et al., 2012, *MNRAS*, 423, 1503  
 Bruntt H. et al., 2010a, *MNRAS*, 405, 1907  
 —, 2010b, *A&A*, 519, A51  
 Claret A., 2000, *A&A*, 363, 1081  
 —, 2004, *A&A*, 428, 1001  
 Collier Cameron A. et al., 2009, *MNRAS*, 400, 451  
 —, 2006, *MNRAS*, 373, 799  
 —, 2007, *MNRAS*, 380, 1230  
 Desidera S. et al., 2004, *A&A*, 420, L27  
 Doyle A. P. et al., 2013, *MNRAS*, 428, 3164  
 Doyle L. R. et al., 2011, *Science*, 333, 1602  
 Enoch B., Collier Cameron A., Horne K., 2012, *A&A*, 540, A99  
 Enoch B., Collier Cameron A., Parley N. R., Hebb L., 2010, *A&A*, 516, A33  
 Faedi F. et al., 2011, *Detection and Dynamics of Transiting Exoplanets*, St. Michel l'Observatoire, France, Edited by F. Bouchy; R. Díaz; C. Moutou; *EPJ Web of Conferences*, Volume 11, id.01003, 11, 1003  
 Ferraz-Mello S., Tadeu Dos Santos M., Beaugé C., Michtchenko T. A., Rodríguez A., 2011, *A&A*, 531, A161  
 Fleming T. A., Schmitt J. H. M. M., Giampapa M. S., 1995, *ApJ*, 450, 401  
 Gillon M. et al., 2011, *A&A*, 533, A88  
 —, 2009, *A&A*, 496, 259  
 Gray D. F., 2008, *The Observation and Analysis of Stellar Photospheres*. Cambridge University Press  
 Hatzes A. P. et al., 2011, *ApJ*, 743, 75  
 Hellier C. et al., 2011, *Detection and Dynamics of Transiting Exoplanets*, St. Michel l'Observatoire, France, Edited by F. Bouchy; R. Díaz; C. Moutou; *EPJ Web of Conferences*, Volume 11, id.01004, 11, 1004  
 Høg E. et al., 2000, *A&A*, 355, L27  
 Howard A. W. et al., 2012, *ApJ*, 749, 134  
 Huélamo N. et al., 2008, *A&A*, 489, L9  
 Jackson A. P., Davis T. A., Wheatley P. J., 2012, *MNRAS*, 422, 2024  
 Jehin E. et al., 2011, *The Messenger*, 145, 2  
 Kovács G., Bakos G., Noyes R. W., 2005, *MNRAS*, 356, 557  
 Kovács G. et al., 2010, *ApJ*, 724, 866  
 Lanza A. F. et al., 2010, *A&A*, 520, A53  
 Lecavelier Des Etangs A., 2007, *A&A*, 461, 1185  
 Lecavelier Des Etangs A. et al., 2010, *A&A*, 514, A72  
 Lendl M. et al., 2012, *A&A*, 544, A72  
 Lucy L. B., Sweeney M. A., 1971, *AJ*, 76, 544  
 Magain P., 1984, *A&A*, 134, 189  
 Mamajek E. E., Hillenbrand L. A., 2008, *ApJ*, 687, 1264  
 Mandel K., Agol E., 2002, *ApJ*, 580, L171  
 Mandell A. M., Drake Deming L., Blake G. A., Knutson H. A., Mumma M. J., Villanueva G. L., Salyk C., 2011, *ApJ*, 728, 18  
 Marigo P., Girardi L., Bressan A., Groenewegen M. A. T., Silva L., Granato G. L., 2008, *A&A*, 482, 883  
 Maxted P. F. L. et al., 2013, *PASP*, 125, 48  
 —, 2011, *PASP*, 123, 547  
 Melo C. et al., 2007, *A&A*, 467, 721  
 Orosz J. A. et al., 2012, *Science*, 337, 1511  
 Pepe F. et al., 2005, *The Messenger*, 120, 22  
 Pollacco D. et al., 2008, *MNRAS*, 385, 1576  
 Pollacco D. L. et al., 2006, *PASP*, 118, 1407  
 Pont F., Aigrain S., Zucker S., 2011, *MNRAS*, 411, 1953  
 Queloz D. et al., 2010, *A&A*, 517, L1+  
 —, 2009, *A&A*, 506, 303  
 —, 2001, *A&A*, 379, 279  
 Saar S. H., Donahue R. A., 1997, *ApJ*, 485, 319  
 Santos N. C. et al., 2003, *A&A*, 406, 373  
 Seager S., Mallén-Ornelas G., 2003, *ApJ*, 585, 1038  
 Sestito P., Randich S., 2005, *A&A*, 442, 615  
 Skrutskie M. F. et al., 2006, *AJ*, 131, 1163  
 Southworth J., 2011, *MNRAS*, 417, 2166  
 Steele I. A., Bates S. D., Gibson N., Keenan F., Meaburn J., Mottram C. J., Pollacco D., Todd I., 2008, in *Society of Photo-Optical Instrumentation Engineers (SPIE) Conference Series*, Vol. 7014, *Society of Photo-Optical Instrumentation Engineers (SPIE) Conference Series*  
 Steele I. A. et al., 2004, in *Society of Photo-Optical Instrumentation Engineers (SPIE) Conference Series*, Vol. 5489, *Ground-based Telescopes*, Oschmann Jr. J. M., ed., pp. 679–692

<sup>1</sup> The data were retrieved from <http://exoplanets.org> on 2013 May 5. See Wright et al. (2011).

- Swain M. R. et al., 2010, *Nature*, 463, 637  
Tamuz O., Mazeh T., Zucker S., 2005, *MNRAS*, 356, 1466  
Torres G., Andersen J., Giménez A., 2010, *A&A Rev.*, 18, 67  
Vidal-Madjar A., Lecavelier des Etangs A., Désert J.-M., Ballester  
G. E., Ferlet R., Hébrard G., Mayor M., 2003, *Nature*, 422, 143  
Voges W. et al., 1999, *A&A*, 349, 389  
Wright J. T. et al., 2011, *PASP*, 123, 412